A diencephalic circuit for opioid analgesia but not positive reinforcement

Maggie W. Waung[1], Kayla A. Maanum[1], Thomas J. Cirino[1], Joseph R. Driscoll[1], Chris O'Brien[2], Svetlana Bryant[2], Kasra A. Mansourian[1], Marisela Morales[3], David J. Barker[2,3], and Elyssa B. Margolis[1,4*]

[1]UCSF Weill Institute for Neurosciences, Department of Neurology, University of California, San Francisco, CA, United States

[2]Department of Psychology, Rutgers University, New Brunswick, NJ, United States

[3]National Institute on Drug Abuse, Neuronal Networks Section, National Institutes of Health, Baltimore, MD, United States

[4]Neuroscience Graduate Program, University of California, San Francisco, CA, United States

*Corresponding Author

Email: Elyssa.Margolis@ucsf.edu

Title- 10; Abstract- 149, Introduction- 332, Results- 2844, Discussion- 1640; Figures- 6, Extended data figures- 8; Tables- 1 Supplementary Table

Abstract

Mu opioid receptor (MOR) agonists are potent analgesics, but also cause sedation, respiratory depression, and addiction risk. The epithalamic lateral habenula (LHb) signals aversive states including pain and we found it is a potent site for MOR-agonist analgesia. Importantly, LHb MOR activation is not reinforcing in the absence of noxious input. The LHb receives excitatory inputs from multiple sites including the ventral tegmental area, lateral hypothalamus, entopeduncular nucleus, and the lateral preoptic area of the hypothalamus (LPO). Here we report that LHb-projecting glutamatergic LPO neurons are excited by noxious stimulation and are preferentially inhibited by MOR selective agonists. Critically, optogenetic stimulation of LHb-projecting LPO neurons produces an aversive state that is relieved by LHb MOR activation, and optogenetic inhibition of LHb-projecting LPO neurons relieves the aversiveness of ongoing pain. Therefore, targeting this MOR sensitive forebrain circuit can relieve pain yet lower the risk of misuse by pain free individuals.

Introduction

Opioids are the most effective pain medications, but the risk of overdose and opioid use disorder limits their clinical utility. Uncoupling the analgesic actions of opioids from those that underlie positive reinforcement is therefore a longstanding goal for pharmacotherapeutic development. Identifying circuits that can drive relief of ongoing pain but not reward in the absence of pain is a critical step towards this goal. The lateral habenula (LHb) may participate in such a circuit, as it is not only activated in a pain setting[1–5] but also by other aversive states including reward omission[6] and animal models of depression[7]. CNS sites involved in pain signaling with reported strong inputs to the LHb include the lateral hypothalamus (LH)[8,9] and anterior cingulate cortex (ACC)[10–12]. Furthermore, efferents from the LHb target pain-responsive regions including the lateral periaqueductal gray, dorsal raphe, parabrachial nucleus, and rostromedial tegmental nucleus[13–15]. While morphine injections that covered a combination

46 of the LHb, medial habenula, and posteromedial thalamus reduce pain-related behavior in an acute pain
47 model[16], whether these effects are due to MOR activation specifically in the LHb is an open question.

48 Since increased activity in LHb neurons encodes aversive states such as ongoing pain, inhibition of this
49 activity should relieve pain. Pain relief, or the mitigation of the aversive state, can produce negative
50 reinforcement[17]. We previously found that MOR activation can decrease neural activity in the LHb via
51 both postsynaptic hyperpolarization and presynaptic inhibition of glutamate release onto subsets of LHb
52 neurons in naïve animals[18]. Here we investigated the specific LHb input circuit and synaptic mechanism
53 by which MOR activation in the LHb produces pain relief. Among six potential inputs to the LHb, we
54 determined that the glutamatergic innervation from the lateral preoptic area of the hypothalamus (LPO) is
55 both pain-responsive and most strongly inhibited by MOR activation. Importantly, we show that
56 activating MORs in this circuit in the absence of pain does not produce reinforcement, suggesting that
57 targeting this circuit could be a significant advance in pain therapy.

58

59 **Results**

60 ***MOR activation in the LHb produces pain relief but not positive reinforcement***

61 To examine the behavioral impact of selective MOR activation in the LHb during ongoing pain, we used
62 the spared nerve injury (SNI) model of persistent neuropathic pain and implanted bilateral cannulae above
63 the LHb in Sprague Dawley rats (Fig. 1a). Hypersensitivity induced by SNI consistently persists for well
64 over one month after induction[19]. We evaluated sensitivity to touch by measuring mechanical stimulation
65 thresholds with graded von Frey filaments. Bilateral microinjections of the MOR-selective agonist
66 DAMGO (10 μM; 300 nL/hemisphere) into the LHb increased the average hindpaw withdrawal threshold
67 compared to saline microinjections in the same animals, specifically in injured animals, indicating that
68 DAMGO reduced the mechanical hypersensitivity generated by SNI in male rats (Fig. 1b; Results of
69 statistical analyses including assumption testing reported in Supplemental Table 1). In contrast, intra-LHb

DAMGO microinjections in sham-injured male rats had no effect on mechanical withdrawal thresholds compared to saline (Fig. 1b). Consistent with the rat literature[19], we did not observe a significant decrease in withdrawal latency to heat in the Hargreaves test after SNI compared to sham-injured controls, and DAMGO microinjections into the LHb did not alter heat withdrawal latency compared to saline in SNI or sham animals (Extended Data Fig. 1a). Intra-LHb DAMGO reversed mechanical hypersensitivity induced by inflammatory pain in the CFA model (Extended Data Fig. 1c-e).

Figure 1

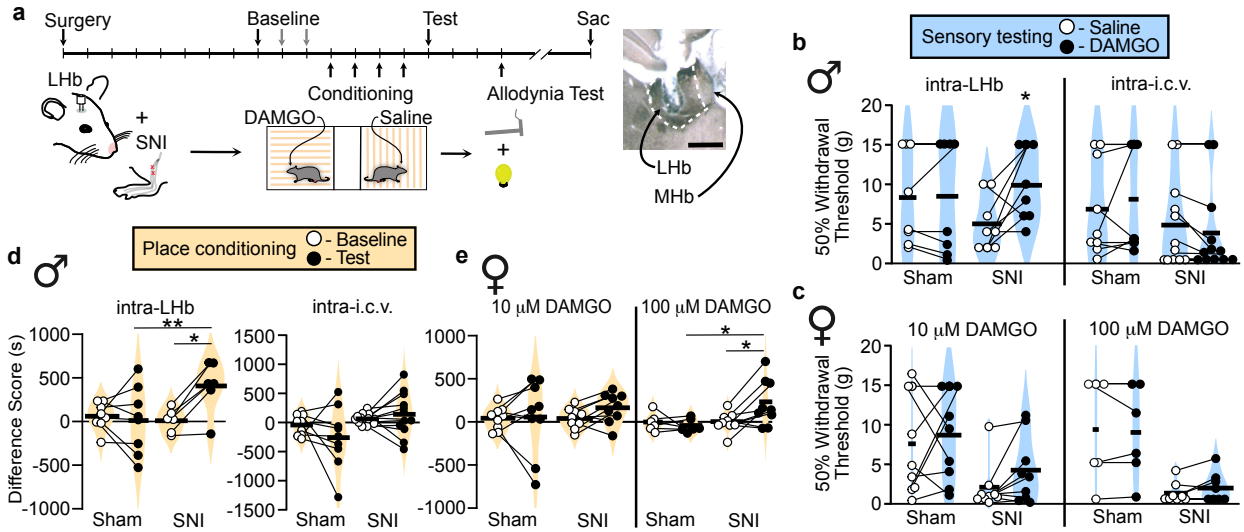

Figure 1. *MOR activation in the LHb relieves allodynia and generates negative reinforcement in rats with neuropathic pain.* **a,** Timeline of behavioral experiments. Right inset, example injection site centered in LHb. Scale bar = 500 μm. **b,** (Left) Violin plots of 50% mechanical withdrawal thresholds following saline or 10 μM DAMGO microinjections into the LHb in sham males (n = 8) and SNI males (n = 8). Assumption testing for statistical analysis is described in Supplemental Table 1. Sham males: Wilcoxon signed rank test, V = 1.5, p =1. SNI males: Wilcoxon signed rank test, V = 2, p = 0.050. (Right) 50% mechanical withdrawal thresholds following saline or 10 μM DAMGO microinjections into the 3rd ventricle (i.c.v.), in male rats with SNI (n = 12) or sham (n = 9) injuries. Sham: Wilcoxon signed rank test, V = 7, p = 0.53. SNI: Wilcoxon signed rank test, V = 31, p = 0.080. **c**, (Left) 50% mechanical withdrawal thresholds following saline or 10 μM DAMGO microinjections into the LHb of sham females (n = 9) or SNI females (n = 9). Bonferroni corrected paired t test, p = 0.703. Wilcoxon signed rank test, V = 7, p = 0.074. (Right) 50% mechanical withdrawal thresholds following saline or 100 μM DAMGO microinjections into the LHb of sham females (n = 6) or SNI females (n = 8). Sham: Wilcoxon signed rank test, V = 5, p = 1. SNI: Wilcoxon signed rank test, V = 6, p = 0.40. **d**, Difference scores in sham males (n = 8) or SNI males (n = 6) before and after conditioning with intra-LHb microinjections of 10 μM DAMGO vs saline. Two-way mixed ANOVA, significant interaction between SNI/sham and baseline/test F(1,13) = 15.93, p = 0.002; post hoc effect group on test day adjusted p = 0.01; paired t-tests, sham

adjusted p = 1; SNI adjusted p = 0.016. (Right) Difference scores in sham males (n = 9) or SNI males (n = 12) before and after conditioning with intra-i.c.v. microinjections of 10 μM DAMGO vs saline: Two-way mixed ANOVA, $F(1,19) = 2.239$, $p = 0.15$. **e,** (Left) Difference scores in sham females (n = 9) and SNI females (n = 9) before and after conditioning with intra-LHb injections of 10 μM DAMGO vs saline. Sham: Bonferroni corrected t-test p = 0.703. SNI: Wilcoxon signed rank test, V = 7, p = 0.07. (Right) Difference scores in sham females (n = 6) and SNI females (n = 9) before and after conditioning with intra-LHb injections of 100 μM DAMGO vs saline. Two-way mixed ANOVA, significant interaction between SNI/sham and baseline/test $F(1,13) = 6.234$, $p = 0.027$; post hoc effect group on test day adjusted p = 0.07; paired t-tests, sham adjusted p = 0.48; SNI adjusted p = 0.035. Means represented by horizontal lines. *$p \leq 0.05$, **$p \leq 0.01$

To evaluate whether MOR activation in the LHb influences the affective experience of pain, we used the place conditioning paradigm in the same group of rats. In a three-chamber apparatus, we paired intra-LHb DAMGO microinjections with one chamber and saline microinjections with the opposite side chamber; the third small chamber served as a neutral area to connect these two. Rats with SNI developed a significant conditioned place preference (CPP) for the LHb-DAMGO-paired chamber, while sham-injured rats did not prefer either chamber following conditioning (Fig. 1d). This indicates LHb-DAMGO is removing an ongoing aversive state producing negative reinforcement rather than producing positive reinforcement via producing a better than expected experience in the absence of a relevant aversive motivational state.

To rule out the potential confound of off-target effects due to DAMGO entering the CSF space via the nearby third ventricle, we microinjected the same solutions intracerebroventricularly (i.c.v.) in male rats with SNI or sham injury. This manipulation did not influence mechanical withdrawal thresholds compared to saline microinjection in either group (Fig. 1b). Furthermore, similar i.c.v. DAMGO microinjections did not generate a CPP in either SNI or sham animals (Fig. 1d). Therefore, we conclude that the behavioral effects of our DAMGO microinjections were due to actions specifically in the LHb.

We also investigated whether LHb MOR activation had the same effects on allodynia and affective pain in female rats. Using the same microinjection parameters as in male rats, female rats with SNI showed a

122 trend towards reduced mechanical allodynia following DAMGO microinjections into the LHb compared
123 to saline (Fig. 1c). Female rats with SNI also showed only a trend towards a preference for the DAMGO-
124 paired chamber (Fig. 1e). As in males, females with SNI displayed no difference in heat withdrawal
125 latency between DAMGO and saline microinjections (Extended Data Fig. 1b). Because female rats may
126 be less sensitive to the analgesic effect of opioids[20,21], we tested a 10-fold higher concentration of intra-
127 LHb DAMGO (100 μM) in a separate cohort of females. This dose was chosen based on studies
128 demonstrating a three-fold reduction in i.c.v. DAMGO antinociceptive efficacy for females in the tail
129 flick test[22]. The higher DAMGO dose induced a significant CPP in female rats with SNI, though still did
130 not reverse mechanical allodynia (Fig. 1c, e). Thus, we conclude that LHb MOR activation can reverse
131 the affective experience of pain in both male and female rats.

132 ***MOR synaptic function persists in LHb neurons in animals with chronic pain***

133 In various CNS regions, chronic pain induces changes in MOR expression and function, including
134 receptor downregulation[23–25]. We previously reported that in naïve male rats MOR activation inhibits
135 glutamate release onto a subset of LHb neurons and also hyperpolarizes approximately 30% of LHb
136 neurons[18]. Here we tested whether these MOR effects are altered in a persistent pain state. To evaluate
137 postsynaptic MOR function we performed whole cell voltage clamp recordings of LHb neurons from
138 acute brain slices from male rats with SNI and measured DAMGO induced changes to holding current
139 (Fig. 2a, b). These responses did not differ from our observations in naïve rats in mean response
140 magnitude (Fig. 2b) or frequency of responsive neurons (two tailed Fisher exact test $p = 1$). We also
141 tested MOR inhibition of glutamatergic electrically-evoked excitatory postsynaptic currents (EPSCs) in
142 LHb neurons from animals with SNI. These responses were also consistent in magnitude and frequency
143 (two tailed Fisher exact test $p = 1$) with observations from naïve rats (Fig. 2c, d). We conclude that these
144 actions of MOR on LHb cell bodies and glutamatergic terminals do not change in animals with ongoing
145 pain.

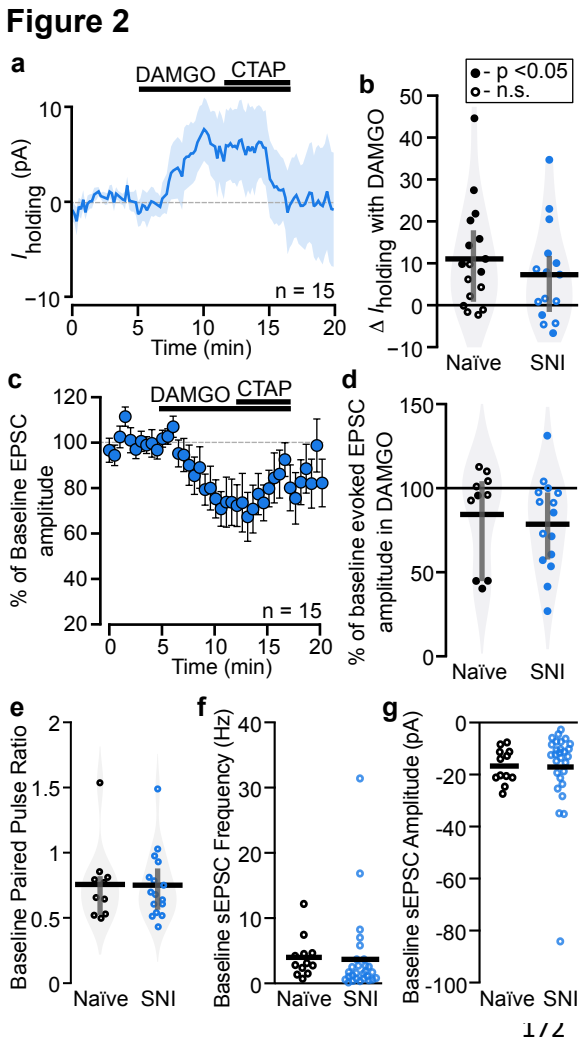

Figure 2. *Ongoing pain does not alter MOR agonist synaptic effects or probability of glutamate release in the LHb.* Responses to the MOR agonist DAMGO were recorded in voltage clamp, V_m = -60 mV. **a**, In animals with SNI, a subset of neurons responded to bath application of the MOR agonist DAMGO (500 nM) with a time locked outward current that was reversed with the MOR selective antagonist CTAP (500 nM). Line indicates mean, shading indicates SEM. **b**, Postsynaptic holding current changes in response to bath application of DAMGO were not different between neurons from naïve and SNI rats: Unpaired t-test df = 29, t = 0.87, p = 0.39. Filled circles indicate cells statistically determined to be "responsive" to DAMGO with within cell unpaired t tests. Grey bars indicate 25th and 75th percentiles. **c**, In rats with SNI, DAMGO (500 nM) induced a time locked inhibition of electrically evoked glutamatergic EPSCs, and CTAP (500 nM) partially reversed the effect. Mean ± SEM. **d**, This DAMGO inhibition of electrically evoked EPSC amplitude was not different between LHb neurons from naïve and SNI rats: Unpaired t-test df = 23, t = 0.47, p = 0.64. Baseline probability of release at glutamatergic synapses was similar between LHb neurons in naïve and SNI rats as measured by (**e**) paired pulse ratio (P2/P1) of electrically stimulated EPSCs (50 ms interstimulus interval): Unpaired t-test, df = 24, t = 0.102, p = 0.92; (**f**) baseline spontaneous EPSC frequency: Unpaired t-test unequal variances, df = 37, t = -0.17, p = 0.87; and (**g**) spontaneous EPSC amplitude: Unpaired t-test unequal variances, df = 38, t = -0.09, p = 0.93. Data from naïve rats previously published in[18].

Increased activity in LHb neurons as well as increased glutamatergic synaptic strength onto LHb neurons are associated with aversive behavioral states[7,26,27]. To evaluate this in LHb neurons from animals with SNI, we evaluated the paired pulse ratio of the electrically evoked EPSCs, a measure of probability of release. There was no difference in paired pulse ratio between groups (Fig. 2e). We next compared the frequency and magnitude of spontaneous glutamatergic EPSCs (sEPSCs) in animals with SNI to those in naïve animals. Mean sEPSC frequency and amplitude were also similar in LHb neurons from SNI and

184 naïve animals (Fig. 2f, g). Together, these observations suggest that painful injury does not induce
185 glutamatergic synaptic plasticity in the LHb.

186 ***The LHb receives functional synaptic input from the LPO, LH, VTA, VP, and EPN, but not the ACC.***

187 LHb neuron firing activity increases with acute noxious stimulation, and an increase in ongoing firing
188 frequency is observed during aversive behavioral states[2,3,7]. In ongoing pain, since we did not observe
189 evidence for changes in glutamatergic synaptic strength, such increases in firing may be driven by greater
190 activity in the glutamatergic axons innervating LHb neurons. Therefore, we hypothesized that the intra-
191 LHb DAMGO-induced behavioral effects that we observed in injured animals were due to MOR
192 inhibition of glutamatergic axon terminals, thus decreasing the aversive excitatory drive onto the LHb
193 neurons. Since MOR activation only inhibits glutamatergic inputs onto a subset of LHb neurons[18], MORs
194 might be preferentially expressed on specific afferent inputs. Prior work characterizing direct functional
195 synaptic connections to the LHb is limited to mice[28], therefore we sought to confirm these functional
196 connections in the rat. We investigated inputs from the entopeduncular nucleus (EPN), lateral preoptic
197 area of the hypothalamus (LPO), and ventral tegmental area (VTA) because stimulating glutamatergic
198 LHb inputs from these sources has been shown to be aversive[26,29,30]. We also investigated inputs from the
199 LH and ACC because they are strongly implicated in pain processing[31], and the VP because stimulating
200 glutamatergic VP neurons increases the firing rate of LHb neurons[32]. We injected AAV2-hSyn-
201 hChR2(H134R)-mCherry into one of these six regions in order to express channelrhodopsin (ChR2) in
202 these different input populations (Fig. 3a). We then made whole cell recordings in LHb neurons and
203 measured light-evoked synaptic inputs while blind to injection site. ChR2 was activated by an LED (λ =
204 473 nm) coupled to an optic fiber placed approximately 100 μm from the recorded cell. Post synaptic
205 currents (PSCs) were measured in response to paired light pulses (1 or 5 ms, 50 ms inter stimulus
206 interval) at holding potentials of -60 mV and -40 mV to probe for EPSCs and $GABA_AR$ mediated
207 inhibitory PSCs (IPSCs) in each cell, respectively. Roughly similar proportions of LHb neurons received
208 synaptic input from each of these targets, with the exception of the ACC where we did not detect any fast

209 PSC connections (Fig. 3b, topographical distribution of connected neurons in Extended Data Fig. 2). The
210 absence of a functional synaptic input from the ACC to the LHb was surprising, as both anterograde[10,12]
211 and retrograde tracers[11] have previously indicated modest inputs. Moreover, the ACC is extensively
212 implicated in behavioral responses to pain and MOR-agonist induced pain relief[33,34]. As a secondary
213 measure of the strength of the innervation, we performed a systematic evaluation of the potential
214 connection using ChR2 as an anterograde tracer, making large injections of AAV2-hSyn-hChR2(H134R)-
215 mCherry throughout the anteroposterior range of the ACC (Extended Data Fig. 3a). This tracing revealed
216 extensive innervation of the nearby mediodorsal thalamus (MDL), but minimal stereologically-quantified
217 fiber labeling in the LHb (Extended Data Fig. 3b, c). Therefore, while we cannot completely rule out a
218 functional input from the ACC to the LHb, any innervation is extremely small compared to the other
219 sources of input to the LHb investigated here.

220 For each brain region from which fast synaptic PSCs were detected in the LHb, both glutamate and
221 GABA inputs were observed in varying proportions (Fig. 3c). Interestingly, while for each input there
222 were individual LHb neurons that received both glutamate and GABA synaptic connections, for each
223 input more than half of the connected LHb neurons received just one type of fast PSC. The VTA was the
224 only input where more LHb neurons received GABAergic synaptic connections than received
225 glutamatergic synaptic connections. Among observed synaptic connections, a wide range of EPSC and
226 IPSC amplitudes were observed for most of the inputs, except for the glutamatergic inputs from the VTA
227 that were consistently small (Extended Data Fig. 4a,c). The delay to light evoked EPSC onset also varied
228 across input source, with LH inputs having the shortest mean latency (Extended Data Fig. 4b).

229

230

231

232

Figure 3

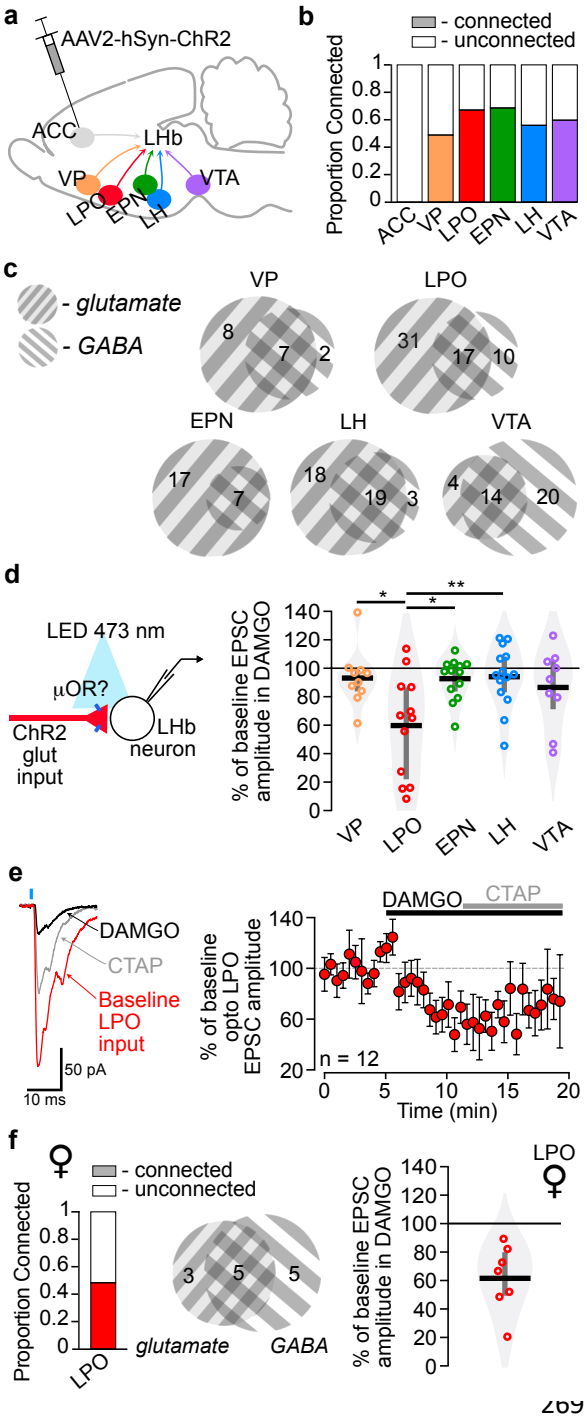

Figure 3. *Glutamatergic inputs to the LHb from the LPO are inhibited by MOR activation.* **a,** Schematic diagram of AAV2-hSyn-hChR2(H134R)-mCherry injection targets which project to the LHb. **b**, Proportions of LHb neurons receiving functional synaptic connections from six input regions measured with optogenetic stimulation of terminals expressing ChR2. **c**, Among connected neurons, venn diagrams depict the numbers of LHb cells receiving optically stimulated glutamatergic and/or GABAergic synaptic input. **d,** (Left) Experiment design: DAMGO (500 nM) was applied during optical synaptic stimulation experiments to probe for functional MOR presynaptic control of glutamate release from specific inputs. (Right) Change from baseline amplitude of optically-evoked EPSCs during DAMGO application. EPSCs from LPO terminal stimulation were most strongly inhibited by MOR activation: One-way ANOVA, df = 4, F = 4.11, p = 0.0057 followed by Tukey HSD pairwise comparisons. **e**, (Left) Representative traces of optically-evoked EPSCs in an LHb neuron from a rat with ChR2 expressed in inputs from the LPO. DAMGO decreased the amplitude of light-evoked EPSC, which was partially reversed by the selective MOR antagonist CTAP (500 nM). Rise time was < 2 ms, indicative of a monosynaptic response. (Right) Summary time course of the DAMGO inhibition across all optically-evoked LPO-LHb EPSCs (n = 12). **f,** LPO inputs to the LHb in female rats (left) had a similar overall connectivity rate but (middle) more GABAergic connections than glutamate connections. (Right) DAMGO inhibited light-evoked glutamatergic synaptic inputs from the LPO to the LHb in female rats as well. *p < 0.05, **p < 0.01

The nature of local LHb neural connections will also impact the circuit's response to MOR activation. There are strong local glutamatergic connections within the LHb[18,35], but there is recent evidence both

273 for[36,37] and against[38,39] the existence of local GABA interneurons. As we only observed somatodendritic
274 MOR responses in a subset of LHb neurons, evidence for GABAergic interneurons in the LHb would
275 impact our model of how MOR activation modulates LHb neural activity, if MOR is preferentially
276 expressed in such interneurons. In the rat, a small number of GAD1 positive neurons are present in the
277 lateral LHb, though these neurons do not co-express vesicular GABA transporter[38], the protein required
278 for loading GABA into synaptic vesicles. In order to detect functional local GABAergic connections
279 within the rat LHb, we injected AAV2-hSyn-hChR2(H134R)-mCherry into the LHb and recorded from
280 LHb neurons. Because some recorded neurons expressed ChR2, we measured light responses before and
281 after application of receptor antagonists in order to isolate the synaptically driven response from the ChR2
282 mediated currents. Under these conditions we did not observe any light activated local IPSCs in LHb
283 neurons (Extended Data Fig. 5). As expected, many neurons received local glutamatergic inputs
284 (Extended Data Fig. 5). We conclude that there is very limited or no local GABAergic interneuron
285 connectivity in the LHb of adult rats.

286 ***MOR activation most strongly inhibits LPO inputs to the LHb***

287 We tested for functional MOR modulation of the light evoked glutamatergic inputs to LHb neurons from
288 each of the regions characterized above. DAMGO induced the strongest and most consistent inhibitions in
289 the terminals arising from LPO neurons (Fig. 3d, e). On average the inhibition was greater in these LPO
290 inputs than the MOR impact on ESPCs observed from the LH, VTA, VP, or EPN (Fig. 3d). We also
291 tested whether MOR inhibits LPO glutamatergic inputs to the LHb independent of sex; the mean
292 inhibition of glutamate release from LPO terminals to LHb neurons in female rats was equivalent to that
293 observed in males (Fig. 3f). Because of the prevalence of local glutamatergic connections in the LHb[18,35]
294 (Extended Data Fig. 5) and postsynaptic MOR inhibition of a subset of LHb neurons[18], we sought to rule
295 out a polysynaptic connection. First, a polysynaptic contribution seems unlikely for the glutamatergic
296 inputs reported here because the delay from light pulse onset to EPSC onset was consistently less than 3
297 ms (Extended Data Fig. 4b). Second, to directly test isolated monosynaptic connections, we expressed

298 ChR2 in LPO neurons and recorded in the LHb; in neurons with light evoked EPSC responses, we
299 applied tetrodotoxin (TTX, 500 nM) and 4-aminopyridine (4 AP; 10 μM). In 8 of 8 tested neurons the
300 light evoked EPSCs persisted in this monosynaptic signal sparing preparation, and this monosynaptic
301 response was inhibited by DAMGO in all 5 tested neurons (Extended Data Fig. 6). Therefore, we
302 conclude that MORs are functionally expressed on LPO terminals that monosynaptically contact LHb
303 neurons, and when these glutamatergic inputs are activated *in vivo*, DAMGO application should inhibit
304 them.

305 ***MOR mRNA is enriched in LHb-projecting LPO neurons***

306 Multiple basal forebrain structures express high levels of MOR including the VP, medial preoptic area
307 (MPO), horizontal diagonal band (HDB), ventral bed nucleus of the stria terminalis (vBNST), and other
308 regions of the extended amygdala complex (EAC)[40]. Some of these not only express MOR to a greater
309 extent than the LPO, but they also project to the LHb. To further evaluate the specificity of MOR
310 expression in LHb-projecting neurons in the LPO compared to nearby brain regions, we performed *in situ*
311 hybridization for MOR mRNA (OPRM1) in brain slices from Sprague Dawley rats where the retrograde
312 tracer Fluoro-Gold had been iontophoresed into the LHb (Fig. 4a - c). With this independent approach,
313 the LHb-projecting LPO neurons showed the strongest OPRM1 expression and contained the greatest
314 number of retrogradely labeled FG(+) neurons co-labeled for OPRM1 (112 ± 9 cells), corresponding to
315 57.1% ± 4.3% of all MOR(+)/FG(+) neurons in the basal forebrain (336/602 total cells). Inputs were also
316 observed from the HDB (23.6% ± 5.9% of MOR(+) cells; 153/602 total cells), VP (9.5% ± 3.1% of
317 MOR(+) cells; 52/602 total cells), MPO (3.0% ± 1.1% of MOR(+) cells; 19/602 total cells), vBNST
318 (3.7% ± 1.2% of MOR(+) cells; 23/602 total cells) and EAC (3.0% ± 2.1% MOR(+) cells; 19/602 total
319 cells; Fig. 4d - f). Overall, these anatomical data are highly consistent with our electrophysiology results,
320 supporting the conclusion that the LPO projection to the LHb is strongly regulated by MORs.

Figure 4

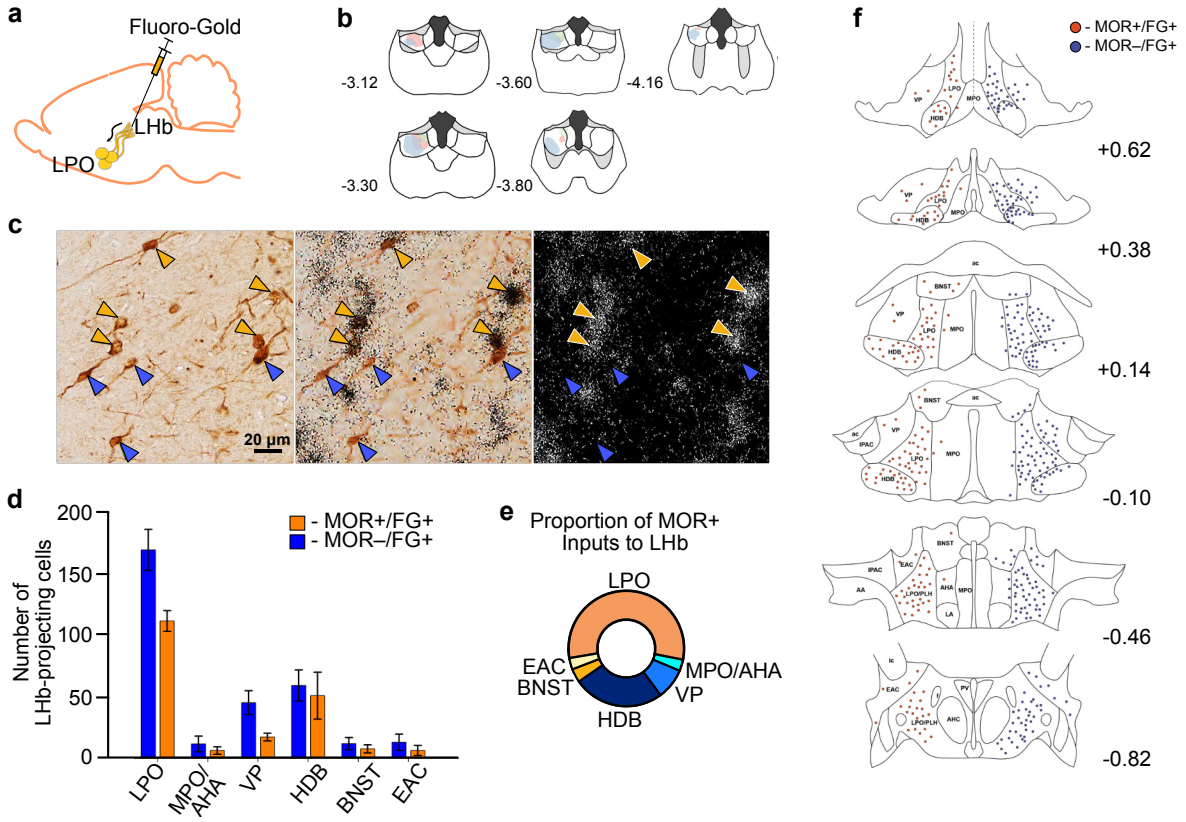

Figure 4. *LPO inputs to the LHb highly express MOR mRNA.* **a,** Schematic of unilateral iontophoretic deposition of the retrograde tracer FG into the LHb. **b**, FG injection sites in LHb (n = 3 rats). **c,** (Left and middle) Representative brightfield images of FG-positive/MOR-positive somas (yellow arrowhead) and FG-positive/MOR-negative somas (blue arrowhead) in the LPO. Scale bar = 20 µm. (Right) Darkfield image of in situ hybridization localization for MOR mRNA (OPRM1). **d,** Number of MOR-positive/FG-positive (yellow) and MOR-negative/FG-positive (blue) cells in various basal forebrain regions. **e**, Donut plot depicting proportions of total MOR-positive inputs to the LHb from various basal forebrain regions. **f,** Locations of FG-positive/MOR-positive (red) and FG-positive/MOR-negative (blue) somata throughout basal forebrain. Co-labeled cells are separated from the singly labelled population for display purposes.

LHb MOR activation blocks the aversiveness of LPO-LHb stimulation

Stimulating LHb-projecting LPO glutamate neurons is aversive in mice[30]. Here we tested whether stimulating the LPO projection to the LHb in rats is aversive with a place conditioning assay. We used an intersectional viral approach injecting the retrograde CAV-Cre into the LHb and AAV2-EF1α-DIO-hChR2(H134R)-mCherry into the LPO bilaterally (Fig. 5a,b). Bilateral optic fibers were implanted above

337 the LPO for laser stimulation of these cell bodies. During conditioning sessions, rats received blue laser
338 stimulation (473 nm, 20 Hz, 5 ms, 10-12 mW) in one environment and no stimulation in the other (Fig.
339 5c). Rats developed a conditioned place aversion to the laser-paired chamber (Fig. 5c).

340 Because ~75% of LHb-projecting LPO neurons in the rat are glutamatergic[30], and because we found that
341 MOR activation inhibits the glutamatergic LPO terminals in the LHb, we hypothesized that the
342 aversiveness produced by stimulating the LHb-projecting LPO neurons should be reduced by MOR
343 agonist injection into the LHb. We tested this by combining the optogenetic intersectional virus
344 manipulation above with behavioral pharmacology through bilateral cannulae aimed at the LHb (Fig.
345 5a,d). During place conditioning sessions rats received either DAMGO or saline into the LHb while also
346 receiving blue light activation of the LHb-projecting LPO neurons in both pairing environments (Fig. 5d,
347 top). Rats with ChR2 expression developed a CPP for the chamber associated with DAMGO, while
348 control mCherry-expressing animals did not (Fig. 5d, bottom). Therefore, MOR activation in the LHb
349 blocked the aversiveness of stimulating the LPO input to the LHb without producing positive
350 reinforcement in the absence of input stimulation.

351 To evaluate the direct contribution of LHb-projecting LPO neural activity to the aversiveness of ongoing
352 pain, we selectively inhibited this circuit connection with the light activated chloride channel iC++ in rats
353 with SNI and a similar intersectional virus approach (Fig. 5f-h). Using *ex vivo* cell attached recordings in
354 LPO neurons expressing iC++ we confirmed that light delivery inhibits action potential firing in these
355 neurons (Fig. 5g). In the place conditioning assay, injured rats developed a preference for the laser-paired
356 chamber but sham rats did not (Fig. 5h). Therefore, decreasing activity specifically in LHb-projecting
357 LPO neurons when an animal is in pain is sufficient to relieve an aversive state and support a CPP.

358

359

360

Figure 5

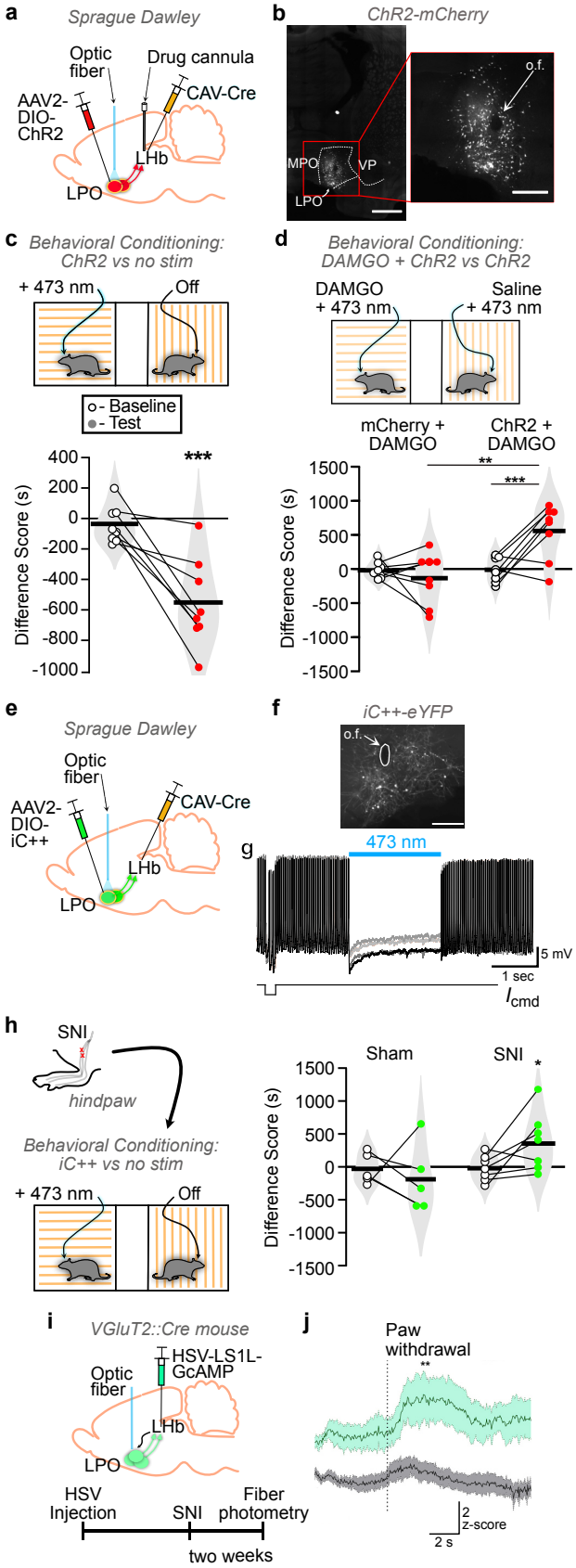

Figure 5. *LHb MOR activation relieves aversiveness of glutamatergic LPO input to the LHb*. **a,** Schematic diagram of dual virus injections to express ChR2-mCherry or mCherry selectively in LPO neurons that project to the LHb, and optic fiber implantation targeting the LPO cell bodies in male rats. **b**, Representative images of Cre-dependent ChR2-mCherry fluorescence in LPO cell bodies. (Left) Scale bar = 250 µm. (Right) Lesion from optic fiber ("o.f.") implant amidst ChR2-mCherry-expressing cell bodies. Scale bar = 50 µm. **c,** Bilateral activation of the LPO-LHb projection in rats (n = 8) produced a robust conditioned place aversion to the stimulation paired side of the place conditioning apparatus (paired t-test, df = 7, t = -4.64, p = 0.002)**. d,** Rats received bilateral blue light stimulation in both conditioning chambers, concomitant with intra-LHb DAMGO in one conditioning chamber or intra-LHb saline in the other. Only animals with active ChR2 (n = 8), but not mCherry controls (n = 8), developed a preference for the intra-LHb DAMGO paired side of the place conditioning apparatus. Two-way mixed ANOVA, significant interaction between ChR2-mCherry/mCherry and baseline/test F(1,14) = 9.982, p = 0.007; post hoc effect group on test day adjusted p = 0.006; paired t-tests, mCherry adjusted p = 0.427; ChR2-mCherry adjusted p = 0.0027. **e**, Schematic diagram of dual virus injections to express iC++-eYFP selectively in LPO neurons that project to the LHb, and optic fiber implantation targeting the LPO cell bodies in male rats that underwent either sham or spared nerve injury. **f**, Representative image of cre-dependent iC++-eYFP fluorescence in LPO cell bodies. Scale bar = 50 µm. **g,** Representative cell-attached recording in current clamp mode of an LPO neurons expressing iC++-eYFP fluorescence, where blue light stimulation paused neuronal firing. **h,** (Left) Rats which had undergone either sham or spared nerve injury two

404 weeks before received bilateral blue light induced inhibition in one chamber or no light in another
405 chamber. (Right) Only animals with spared nerve injury (n = 7), but not sham injury (n = 5) developed a
406 preference for the blue light paired side of the place conditioning apparatus. Two-way mixed ANOVA,
407 trending interaction between sham/spared nerve injury (SNI) and baseline/test $F(1,10) = 3.443$, $p = 0.093$;
408 post hoc paired t-tests for sham adjusted $p = 0.580$; spared nerve injury (SNI) adjusted $p = 0.048$. **i,**
409 Schematic diagram of HSV-hEF1α-LS1L-GCaMP6m injection into the LHb of VGluT2::Cre mice, to
410 induce expression of GCaMP6m in glutamatergic LPO neurons innervating the LHb, and optic fiber
411 implant for fiber photometry imaging in the LHb-projecting LPO neurons. (Right) Experimental timeline.
412 **j**, Mice with SNI (green, n = 5) exhibited significantly larger changes in GCaMP6m fluorescence time-
413 locked to paw withdrawal in response to thermal stimulation in the Hargreaves apparatus compared to
414 sham controls (grey, n = 9): Two-way ANOVA, $F(1,12) = 5.439$, $p = 0.038$; Holm-Sidak post-hoc test, p
415 = 0.0074. *$p < 0.05$, **$p < 0.01$, ***$p < 0.005$

416

417 ***Noxious stimulation activates glutamatergic LHb-projecting LPO neurons***

418 Finally, we tested whether glutamatergic LHb-projecting LPO neurons are activated by noxious
419 stimulation and whether ongoing pain alters this response. We expressed the calcium indicator
420 GCaMP6m in LHb-projecting LPO neurons using a Cre-dependent, retrograde viral construct HSV-
421 hEF1α-LS1L-GCaMP6m injected to the LHb of VGluT2::Cre mice (Fig. 5i). We implanted optic fibers
422 above the LPO in control and SNI mice and performed fiber photometry prior to and during noxious heat
423 stimulation. On average, GCaMP6m signal increased as paw withdrawal commenced, and this response
424 was greatly potentiated in mice with SNI (Fig. 5j), who also displayed shorter withdrawal latencies to heat
425 (Extended Data Fig. 7). Thus, glutamatergic LPO neurons that project to the LHb are activated in
426 response to noxious peripheral stimulation, and the magnitude of activation is greater during ongoing
427 pain.

428

429 **Discussion**

430 Here we identified a circuit that can be targeted by MOR agonists to relieve the aversiveness of ongoing
431 pain but does not produce reward in pain free rodents (Fig. 6). MOR agonist action in the LHb was
432 sufficient to reverse injury-induced allodynia and to produce a CPP, decreasing both sensory and affective

433 pain responses, respectively. Importantly, sham-injured animals did not develop a CPP, indicating that
434 MOR activation in the LHb does not produce positive reinforcement in the absence of pain.
435 Unexpectedly, rather than inputs from brain regions previously established as mediating pain and opioid-
436 induced pain relief, it is the glutamatergic inputs from the LPO that we demonstrate are preferentially
437 controlled by LHb MOR activation. We found that the aversiveness produced by optogenetic activation of
438 LHb-projecting LPO neurons is blocked by MOR agonist microinjection into the LHb. Importantly,
439 optogenetic inhibition of this circuit in injured animals produced place preference, parallel to LHb MOR
440 activation and indicating that inhibiting LHb-projecting LPO neurons is sufficient to relieve the ongoing
441 aversive state. Together, these experiments show that MOR activation in the LHb can generate negative
442 reinforcement via pain relief, but not positive reinforcement in the absence of noxious stimuli.

Figure 6

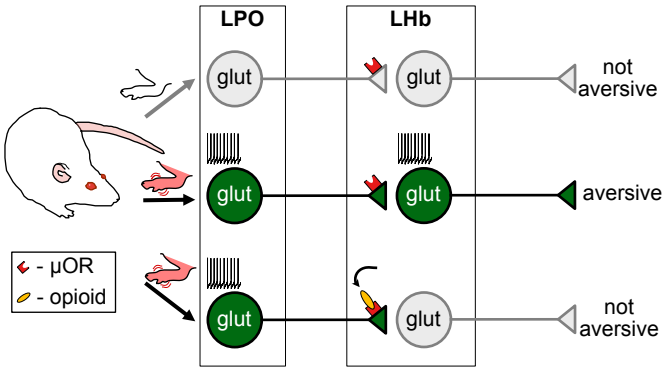

Figure 6. Summary: LHb-projecting LPO glutamatergic neurons that fire more during pain provide an aversive signal. MOR activation in the LHb inhibits the glutamate release from the LPO, preventing propagation of the aversive signal further in the circuit.

452 ***The LHb in pain and relief***

453 The LHb plays a role in the perception of noxious stimuli in injury and depression models[41,42], and most
454 LHb neurons have increased firing rates during aversive behavioral states and in response to noxious
455 stimuli[2,3]. Bilateral lesions of the LHb decrease hypersensitivity to touch generated by the chronic
456 constriction ischemia model of neuropathic pain in rats[43], supporting the notion that signaling through the
457 LHb contributes to injury-induced mechanical allodynia. In the aversive state of alcohol withdrawal,
458 chemogenetic inhibition of the LHb relieves thermal hyperalgesia[41]. We found that LHb MOR activation
459 reverses mechanical hypersensitivity in a model of neuropathic pain in males but not significantly in

460 females. In place conditioning measures, in a design used to evaluate the impact of a manipulation on the
461 affective component of pain, we observed that intra-LHb DAMGO induced a CPP in both males and
462 females with ongoing pain, but not in shams of either sex. Female rats required a higher concentration of
463 DAMGO to produce intra-LHb CPP, consistent with prior studies showing that across rodent strains
464 females show less opioid induced antinociception than males[44,45]. Together these observations support the
465 model that LHb neural activity increases in aversive behavioral states and manipulations that decrease
466 that firing provide a relief signal.

467 We previously discovered two potential mechanisms by which MOR activation inhibits LHb neural
468 activity: presynaptic inhibition of glutamate release or postsynaptic outward current generation in a subset
469 of LHb neurons[18]. Here we found that these two MOR effects are intact in animals with ongoing pain.
470 Because the behavioral effect of LHb MOR activation was specific to injured rats we hypothesized that in
471 control conditions the MOR sensitive LHb circuit elements have low activity levels and this activity
472 increases in ongoing pain. Since DAMGO induced outward currents in LHb neurons are modest and
473 DAMGO induced inhibition of glutamate release onto a subset of LHb neurons was quite strong, we
474 further hypothesized that there is increased glutamatergic drive to the LHb in the pain state, in an input
475 that is MOR sensitive.

476 The vast majority of LHb neurons are glutamatergic, and there is anatomical evidence for dense bouton-
477 like structures arising from local LHb neurons[46]. This local feed forward connectivity may distribute a
478 specific excitatory LHb input across the various LHb projections that include the dorsal raphe,
479 ventrolateral PAG, MDL, centromedian thalamus, LH, RMTg, and VTA[9,13,14,47]. Local connectivity has
480 also been observed with functional assays, including that TTX application decreases the frequency of
481 sEPSC and sEPSP events in a subset of LHb neurons[18,35] and that optogenetic activation of LHb neurons
482 induces glutamatergic EPSCs (Extended Data Fig. 5). This feed forward circuit enables the distribution of
483 an afferent excitatory signal across LHb neurons, and it raises the possibility that inhibition of such an
484 input by a MOR agonist will decrease activity in many LHb projection neurons, even those that are not

485 directly innervated by the excited pathway. Therefore, it is possible that MOR inhibition of one specific
486 glutamatergic input, such as the LPO, can decrease the distribution of an excitatory drive onto many
487 efferent LHb projections.

488 We characterized the functional glutamatergic connections from a variety of brain regions to the LHb in
489 rats; our findings are largely consistent with prior reports utilizing similar techniques in mice. Still, we
490 note that outcomes of these experiments are dependent on the types and number of neurons that express
491 ChR2 following the virus injections and are limited by the geometry of an injection site. We detected the
492 strongest glutamatergic inputs from the LH and EPN, while glutamatergic synaptic responses from the
493 VTA were quite small. We found no functional inputs from the ACC, and in a systematic anatomical
494 analysis we detected very few afferent fibers from the ACC present in the LHb. Of the detected
495 glutamatergic inputs, we expected brain regions associated with pain perception and pain relief, such as
496 the LH and VTA, to be more strongly modulated by MOR activation. However, we instead found MOR
497 mRNA and function were clearly enriched in LPO inputs to the LHb.

498 Because LHb neurons generally fire more in response to noxious stimuli, and optogenetic stimulation of
499 various glutamatergic inputs to the LHb is uniformly aversive[27,29,30,48,49], we hypothesized that a
500 glutamatergic input to the LHb transmits the pain signal. Further, aversive stressors lead to an increase in
501 the ratio of excitatory glutamatergic to inhibitory GABAergic in synaptic input to LHb neurons[48–50], and
502 restoration of this ratio is associated with relief of aversive states such as foot shock-induced learned
503 helplessness[49] and cocaine withdrawal[48]. Therefore, a pharmacological manipulation that decreases the
504 excitatory drive onto LHb neurons should also relieve aversive states. Because we found that DAMGO in
505 the LHb generates CPP only in animals with ongoing pain, our data suggest a MOR-sensitive
506 glutamatergic input to the LHb is active during pain and relatively inactive in the absence of pain.

507 ***The LPO: a brain region contributing to pain perception***

508 The LPO projection to the LHb is composed of neurons releasing either glutamate or GABA; these
509 neurons do not co-release glutamate and GABA[30], unlike other LHb inputs[51]. Optogenetic activation of
510 LPO glutamate projections to the LHb is aversive in mice[30], and here we posited that this activation
511 mimics an ongoing pain signal. We found in rats that stimulating the LPO inputs to the LHb even without
512 isolating the glutamatergic component is also aversive. This is consistent with our electrophysiology
513 observations that the glutamate component of this projection appears stronger than the GABAergic
514 component in our preparations. Isolated activation of the VGaT LHb-projecting LPO neurons generates a
515 place preference[30], thus stimulating both populations of neurons in rats here may generate a weaker
516 aversion than selective activity in the glutamatergic component of the connection. However, GCaMP6s
517 recordings in transgenic mice show that activity increases in response to an aversive stimulus and its
518 predictive cue in both VGaT and VGluT2 LPO neurons that project to the LHb[30], therefore stimulating
519 both inputs may have some relation to *in vivo* activity patterns. We were able to relieve the aversiveness
520 of activation of this connection with a MOR agonist in the LHb. Further, inhibiting the LPO projection to
521 the LHb specifically in injured animals was sufficient to produce a CPP. While a causal role for the LPO
522 in pain perception is unexplored to date, anterograde[52] and retrograde[53] tracing has shown a direct input to
523 the LPO from the spinal cord. Also, injections of the pro-inflammatory cytokine IL-1ß into the LPO
524 induces hyperalgesia, indicating LPO participation in a nociception circuit[54]. Painful stimuli such as
525 subcutaneous formalin injections, mild electric shock, and tail pinch also increase firing in some LPO
526 neurons[55,56]. Here we show that glutamatergic LPO projections to the LHb increase their activity in
527 response to noxious stimulation and that the magnitude of this response is greater in animals with ongoing
528 pain. This combined with our optogenetic manipulations indicate that a major output for LPO pain signals
529 is to the LHb.

530 ***The LPO to LHb circuit: A unique target for analgesia***

531 Opioids remain the best available clinical analgesics, yet systemically administered opioids can result in
532 serious adverse consequences including opioid use disorder and respiratory depression[57]. Opioid-induced
533 positive reinforcement and euphoria, combined with the development of dependence, underlie opioid
534 abuse liability. To date, there is little clinical evidence that the analgesic and euphoric effects of opioids
535 can be decoupled in humans, yet this possibility is a potential pathway to improve therapies for pain. Here
536 we have identified a key circuit whose modulation relieves pain but does not generate reward in the
537 absence of pain. This dissociation between relief and reward provides a neural target for pain treatment
538 without promoting substance use disorder. Is it possible to activate MORs in the LHb but not in a reward
539 circuit? There is some preclinical evidence that this dissociation is possible by developing MOR ligands
540 with the appropriate opioid pharmacology. For example, a novel, cyclized, stabilized MOR selective
541 agonist based on endomorphin I produces pain relief but not reward[58]; a similar pattern has been observed
542 for analogs of mitragynine[59]. An alternative approach would be to target a different receptor with high
543 expression levels in this circuit in a way that would decrease LHb neural activity. Relevant to this
544 approach, mRNA expression for a selection of orphan G-protein coupled receptors (GPCRs) is enriched
545 in the habenula[39,60,61]. One such receptor is GPR151, and LHb neurons containing GPR151 receive input
546 from the LPO[62]. Such directed strategies present a range of new anatomic and molecular targets for pain
547 therapy. By identifying the LPO-LHb connection as a site able to provide relief from neuropathic pain
548 and injury-induced allodynia, we have discovered a unique circuit that may achieve effective opioid-
549 mediated pain relief independent of the drug's addictive properties.

550

551 **Online Methods**

552 ***Animals***

553 All experiments were performed in accordance with the guidelines of the National Institutes of Health
554 Guide for the Care and Use of Laboratory Animals and the Institutional Animal Care and Use
555 Committees (IACUC) at the University of California San Francisco, the National Institute on Drug Abuse
556 (NIDA), and Rutgers University.

557 Male and female Sprague Dawley rats were obtained from Charles River Laboratories. Rats were allowed
558 access to food and water *ad libitum* and maintained on a 12h:12h light/dark cycle. Rats used in behavioral
559 and *in situ* hybridization studies were housed under reverse light/dark cycle conditions. Rats were group
560 housed until they underwent surgery, after which they were singly housed.

561 Male and female VGluT2::Cre mice were bred from mice obtained from the Jackson Laboratory (Jax #
562 016963). Mice were allowed access to food and water *ad libitum* and maintained on a 12h:12h light/dark
563 cycle with lights on at 7 AM. Mice were always housed in groups of 2-5.

564 ***Viral constructs***

565 AAV2-hSyn-hChR2(H134R)-mCherry (titer: 2.9e+12), AAV2-hSyn-mCherry (titer: 4.7e+12), and
566 AAV2-EF1α-DIO-ChR2-mCherry (titer: 5.1e+12), and AAV2-Ef1α-DIO-iC++-eYFP (titer: 5.9e+12)
567 were purchased from the University of North Carolina Vector Core with available stock constructs from
568 the laboratory of K. Deisseroth at Stanford University. CAV-Cre (titer: 2.5e+12) was purchased from
569 Montpelier University, France. HSV-hEF1α-GCaMP6m (titer: 5e+9) was purchased from the Gene
570 Delivery Technology Core at Massachusetts General Hospital.

571 ***Stereotaxic injections***

572 Rats weighing 275-300 g were anesthetized with 3-5% isoflurane (Henry Schein) via inhalation and
573 secured in a stereotaxic frame. Bilateral craniotomies were created with a dental drill above the injection

site. For electrophysiology experiments, injections of AAV2-hSyn-hChR2(H134R)-mCherry were made bilaterally into the LPO (-0.3 mm anteroposterior (AP), ±1.4 mm mediolateral (ML), -8.4 mm dorsoventral (DV)), VP (-0.24 mm AP, ±2.6 mm ML, -7.8 mm DV), EPN (-2.4 mm AP, ±3.0 mm ML, -7.0 mm DV), LH (-2.6 mm AP, ±1.7 mm ML, -8.2 mm DV), VTA (-5.8 mm AP, ±0.5 mm ML, -8.5 mm DV), anterior ACC (+2.2 mm AP, ±0.6 mm ML, -2.6 mm DV), or posterior ACC (+1.7 AP, ±0.6 mm ML, -2.6 mm DV) using a Nanoject II (Drummond Scientific, Broomall, PA). A volume of ~500-830 nL was injected per hemisphere over a period of 4.5 min. The glass injector tip was left in place for at least 2 additional minutes before slow withdrawal to prevent backflow and infection of tissue dorsal to the injection target.

For optogenetic behavior experiments, AAV2-EF1α-DIO-hChR2(H134R)-mCherry, AAV2-EF1α-DIO-mCherry, or AAV2-EF1α-DIO-iC++-eYFP were injected into the LPO as above and CAV-Cre was injected bilaterally into the LHb (-3.6 mm AP, ±0.65 mm ML, -5.4 mm DV) with a microinjector connected via polypropylene tubing to Hamilton syringes controlled by a dual syringe pump (KD pump) guided by a bilateral 33G stainless steel guide cannula (Plastics One).

Rats were treated with subcutaneous Carprofen (5 mg/kg, Zoetis) and topical 2% Lidocaine (Phoenix Pharmaceutical, Inc.) during the surgery for pain control. After surgery, animals had access to liquid Tylenol (~1:40) in their drinking water for 3-5 days or were administered Meloxicam (s.c. 2mg/kg, Pivetal) once per day for two days.

Cannulation and optic fiber implantation

Two to four weeks after virus injection, rats slated for behavioral testing underwent a second cranial surgery to implant custom-made 200 μm optic fibers at a 5° angle of rotation in the coronal plane into the bilateral LPO (-0.6 mm AP, ± 3.05 mm ML, -7.5 mm DV). For microinjections into the LHb, bilateral guide cannulae were implanted 1 mm above the LHb (-3.7 mm AP, ± 0.65 mm ML, -4.4 mm DV). A dummy stylet was inserted to maintain patency of the cannulae. Optic fibers and cannulae were anchored

598 with flat point screws and dental cement. For i.c.v. microinjections, unilateral cannulae were implanted
599 into the right lateral ventricle (-1.0 mm AP, + 1.5 mm ML, -3.5 mm DV).

600 Analgesia during surgery and recovery was administered as described above. Animals were allowed to
601 recover for 1-2 weeks prior to behavioral testing. All virus injections, optic fiber placements, and
602 cannulae placements were histologically verified postmortem based on the standard rat brain atlas[63].

603 ***Spared nerve injury***

604 Spared nerve injury (SNI) of the sciatic nerve branch was performed to model chronic neuropathic pain[19].
605 Under isoflurane anesthesia, a 2-cm skin incision was made over the left hindlimb. The biceps femoris
606 muscle was blunt dissected to expose the branches of the sciatic nerve. The common peroneal and tibial
607 nerves were ligated with 5.0 silk surgical suture and transected distally, with sparing of the sural nerve
608 branch. For sham procedures, a skin incision was made and biceps femoris muscle was exposed without
609 dissection. The overlying skin was closed with a monocryl suture. Animals were allowed seven days to
610 recover from surgery prior to behavioral testing. Behavioral indications of ongoing pain such as paw
611 guarding were observed in all animals used in the SNI groups.

612 ***Inflammatory pain model***

613 Peripheral inflammation was induced using Complete Freund's Adjuvant (CFA; Sigma Life Science).
614 Under isofluorane anesthesia, a 1:1 emulsion of CFA and sterile saline (150 μL) was injected into the
615 footpad of the rat's left hindpaw with a 27 G needle. Sham-injured controls were injected with sterile
616 saline (150 μL).

617 ***Microinjections***

618 Rats were lightly restrained in a cloth wrap for intracranial microinjections. A bilateral 33G microinjector
619 (PlasticsOne) that extended 1 mm ventrally beyond the guide cannula was inserted to target drug delivery
620 into the LHb or i.c.v. Hamilton syringes were driven by a dual syringe pump to infuse either vehicle

621 (phosphate buffered saline, PBS) or DAMGO (10 μM, 300 nL/hemisphere administered over 2 min). A
622 separate cohort of female rats was microinjected with 100 μM DAMGO.

623 ***von Frey sensory assessment***

624 Standard von Frey sensory assessments were performed as described[64]. Briefly, rats were habituated to
625 sensory testing chambers (Plexiglass boxes with mesh-like flooring) for at least 2 days prior to testing.
626 Behavioral assessments did not begin until exploratory behavior subsided. Testing was completed with
627 eight Touch Test ® fibers (North Coast Medical & Rehabilitation Products, Gilroy, CA, USA) ranging
628 from 0.4 to 15 g. Fibers were pressed perpendicularly to the mid-plantar left hindpaw with sufficient force
629 to cause bending in the fiber and held for 3-4 s. A positive response was noted if the paw was sharply
630 withdrawn. Ambulation was not considered a positive response. When responding was ambiguous, testing
631 was repeated. 50% withdrawal thresholds were calculated using fiber application in ascending stiffness
632 order or using the up down method.

633 In behavioral pharmacology experiments rats underwent sensory testing 5 min after counterbalanced
634 saline or DAMGO microinjections on the same day, with at least 4 h between infusions. Experimenters
635 were blinded to the solution composition during administration and testing.

636 ***Hargreaves sensory assessment***

637 Hargreaves tests were completed in sensory testing chambers with glass flooring. Assessment
638 commenced after rats acclimated to the chamber. Testing was completed using a plantar test analgesia
639 meter (Series 8 Model 390, IITC Life Science, Woodhills, CA, USA). Radiant light was directed toward
640 the mid-plantar left hindpaw until a sharp paw withdrawal response was observed with a 30 s maximum
641 cutoff. Ambulation was not considered a positive response. At baseline testing, measurements were
642 repeated at different intensity levels until the average withdrawal latency of eight trials was 15 ± 2 s.
643 Subsequent measurements were performed using this individualized intensity level.

644 ***Place conditioning***

645 Conditioned place preference (CPP) pairings occurred twice daily for four consecutive days following the
646 post-surgery sensory tests with DAMGO and saline. The conditioning boxes (Med. Associates, Georgia,
647 VT, USA) have 3 divisions: two conditioning chambers (25 cm x 21 cm x 21 cm) with distinct visual
648 (horizontal vs. vertical stripes) and textural (thick vs. thin mesh flooring) cues, separated by a third,
649 smaller gray neutral chamber (12 cm x 21 cm x 21 cm). Before conditioning commenced, animals were
650 allowed up to three opportunities to show neutrality across the chambers during 30-minute baseline
651 sessions. Rats that displayed a consistent baseline preference (>65% of time spent in one chamber) were
652 excluded from the study. Rats were pseudorandomly assigned to receive DAMGO in one of the
653 conditioning chambers, and assignments were counterbalanced for each cohort.

654 During conditioning sessions, microinjections were performed as described above through the intra-LHb
655 cannulae just before the rat was confined to the designated chamber for 30 min. Morning and afternoon
656 pairing sessions were at least 4 h apart and the order of pairings was alternated on each conditioning day.
657 On test day, rats were allowed to freely explore the chambers for 30 min and time spent (s) in each
658 partition was recorded. Difference score was defined as (Time spent in DAMGO-paired chamber) - (Time
659 spent in saline-paired chamber).

660 For ChR2 activation studies, rats were acclimated to handling and attachment of fiber cables to fiber
661 implants in a neutral environment. On procedure days, fiber implants were connected to optic fiber cables
662 attached to a 1x2 fiber optic rotary joint (Doric Lenses, Quebec, Canada). A laser light source (MBL 473,
663 OEM Laser Systems, East Lansing, MI) was adjusted to deliver 80-120 mW/mm light intensity at the end
664 of the fiber implant[2]. Light stimulation (5 ms pulses at 20 Hz) commenced upon placing rats into the
665 designated chamber of a custom built three chamber box on conditioning days. During baseline and
666 testing sessions, the time spent in each chamber was recorded using a webcam and analyzed using Viewer
667 software (Biobserve, Bonn, Germany).

668 ***Brain removal and immunohistochemistry***

669 Rats were deeply anesthetized with an intraperitoneal injection of Euthasol (0.1 mg/kg, Virbac Animal
670 Health, Fort Worth, TX) after 0.3 µl of Chicago Sky Blue (in 2% PBS) was injected through the cannulae
671 to mark injection locations. After becoming unresponsive to noxious stimuli, the rats were transcardially
672 perfused with 400 mL of saline, followed by 400 mL of 4% paraformaldehyde (PFA) in 0.1 M phosphate
673 buffer. The brains were extracted and immersion-fixed in PFA for 2 h at room temperature (RT), washed
674 two times with PBS to remove excess PFA, and stored in 1X PBS at 4ºC until they were sectioned (50
675 µm) using a vibratome (Leica VT 1000 S). Sections were mounted on slides using VECTASHIELD ®
676 mounting medium (Vector Laboratories, Burlingame, CA, USA). Images were taken under a Zeiss Stemi
677 2000-C (Pleasanton, CA) using an Amscope MD800E running AmScope x64 3.0 Imaging Software.

678 To label biocytin filled cells after slice electrophysiology recordings, slices were washed three times for 5
679 min each with PBS (Gibco, Waltham, MA), then blocked with a solution containing: bovine serum
680 albumin (0.2%), normal goat serum (5%) and Tween20 (0.3%; Sigma-Aldrich, St. Louis, MO) for 2 h at
681 RT. Slices were incubated in DTAF-streptavidin (1:200; Jackson Immuno Research) diluted in PBS +
682 0.3% Tween20 for 48 h at 4° C. After five, 10-min rinses, brain slices were mounted onto glass slides as
683 above and imaged using a Zeiss Axioskop upright microscope (2.5X, NA = 0.075 or Plan Apochromat
684 20X, NA = 0.75).

685 ***Electrophysiology***

686 Rats were deeply anesthetized with isoflurane, decapitated, and brains were quickly removed into ice-cold
687 artificial cerebrospinal fluid (aCSF) consisting of (in mM): 119 NaCl, 2.5 KCl, 1.0 NaH_2PO_4, 26.2
688 $NaHCO_3$, 11 glucose, 1.3 $MgSO_4$, 2.5 $CaCl_2$, saturated with 95% O_2-5% CO_2, with a measured osmolarity
689 310–320 mOsm/L. Two hundred µm coronal sections through the LHb were cut with a Leica VT 1000 S
690 vibratome. Tissue containing the virus injection sites was drop fixed in 10% formalin. Slices were
691 incubated in oxygenated aCSF at 33 °C and allowed to recover for at least one hour. A single slice was

692 placed in the recording chamber and continuously superfused at a rate of 2 mL/min with oxygenated
693 aCSF. Neurons were visualized with an upright microscope (Zeiss AxioExaminer.D1) equipped with
694 infrared-differential interference contrast, Dodt optics, and fluorescent illumination. Whole cell
695 recordings were made at 34°C using borosilicate glass microelectrodes (3-5 MΩ) filled with K-gluconate
696 internal solution containing (in mM): 123 K-gluconate, 10 HEPES, 8 NaCl, 0.2 EGTA, 2 MgATP, 0.3
697 Na_3GTP, and 0.1% biocytin (pH 7.2 adjusted with KOH; 275 mOsm/L). Liquid junction potentials were
698 not corrected during recordings. Input and series resistance were monitored throughout voltage clamp
699 experiments with a −4 mV step every 30 seconds. Series resistance was required to be 5-30 MΩ and cells
700 with series resistance changes > 25% were excluded.

701 Signals were recorded using a patch clamp amplifier (Axopatch 1D, Molecular Devices, San Jose, CA or
702 IPA, Sutter Instruments, Novato, CA). Signals were filtered at 5 kHz and collected at 20 kHz using IGOR
703 Pro (Wavemetrics) or collected at 10 kHz using SutterPatch software (Sutter Instruments). Light evoked
704 EPSCs and IPSCs were evoked by two blue light pulses (473 nm, 1-10 ms) administered 50 ms apart,
705 once every 30 s. LHb recordings were generally made in LHb subregions enriched in ChR2-expressing
706 fibers. Recordings were made in voltage-clamp mode, with membrane potential clamped at $V_m = -60$ mV
707 and −40 mV, for EPSCs and IPSCs respectively. Light was delivered by an LED coupled to an optic fiber
708 aimed at the recorded cell (7-10 mW). To calculate connectivity rates, only the first neuron patched per
709 slice was included in order to avoid over sampling from slices or animals with lower infection rates. All
710 measurements of DAMGO effects on EPSCs were completed in the presence of gabazine. After
711 recordings, slices were drop fixed in 4% PFA for at least 2 h at 4°C and processed for biocytin labeling.

712 *Data analysis for electrophysiology*. Light pulses were considered to reveal synaptic connections when
713 three conditions were met: (1) the average of 8 traces showed a deviation from baseline $I_{holding}$ such that
714 the mean trace exceeded 4 SD of 10 ms baseline period within the 10 ms window after initiation of light
715 pulse, (2) the putative response was observed in at least 3 independent trials, and (3) the delays from the
716 light stimulation onset of putative responses were time locked (<1 ms jitter) across trials. Latency was

717 calculated as time from start of light pulse to when the rate of rise exceeded −40,000 V/s. In some cases
718 DNQX (10 μM) or gabazine (10 μM) was bath applied to confirm inward and outward currents as AMPA
719 receptor or $GABA_A$ receptor-mediated, respectively. The magnitude of DAMGO induced changes were
720 quantified by comparing the mean values over the last 4 min of DAMGO application to the 4 minutes of
721 baseline just prior to starting the DAMGO application. Where individual neurons were evaluated for
722 significant responses, DAMGO sensitive neurons were identified by comparing 30 sec binned samples
723 during these two time windows with an unpaired t-test.

724 ***Combined retrograde tracing and* in situ *hybridization***

725 *Tracer injections*. Male Sprague Dawley rats (300-500 g) were anesthetized with 2-5% isoflurane. 1%
726 Fluoro-Gold (FG; FluoroChrome LLC) solution in a 0.1M cacodylate buffer (pH 7.5) was delivered
727 unilaterally into the LHb (−3.4 mm AP, ± 0.9 mm ML, and −5.4 mm DV) iontophoretically through a
728 stereotaxically positioned glass micropipette (18-25 μm inner diameter) by applying 1 μA, 7 s pulses at
729 14 s intervals for 20 min. The micropipette was then left in place for an additional 10 min to prevent
730 backflow. Following surgery, rats were singly housed and perfused 3 weeks later.

731 *Tissue Preparation.* Rats were anesthetized with chloral hydrate (0.5 ml/kg) and perfused transcardially
732 with 4% (w/v) PFA in 0.1M phosphate buffer treated with diethylpyrocarbonate (DEPC), pH 7.3. Brains
733 were post-fixed in 4% PFA for 2 h before being transferred to an 18% sucrose solution (w/v in 0.1M
734 PBS) and stored overnight at 4°C. Coronal sections of the LHb (30 μm) and LPO (16 μm) were prepared.

735 *Phenotyping of retrogradely labeled cells by immunocytochemistry and in situ hybridization.* Sections in
736 the LPO were incubated for 2 h at 30°C with rabbit anti-FG antibody (1:500; AB153; Millipore)
737 supplemented with RNAsin. Sections were then incubated in biotinylated goat anti-rabbit antibody
738 (1:200; BA1000; Vector Laboratories) for 1 h at 30 °C. Sections were then rinsed and treated with 0.2N
739 HCl, rinsed, and then acetylated in 0.25% acetic anhydride in 0.1 M triethanolamine. Subsequently,

740 sections were rinsed and post-fixed with 4% PFA, rinsed, and then incubated in a hybridization buffer for
741 2 h at 55°C.

742 Hybridization was then performed for radioactive detection of MOR mRNA by hybridizing sections for
743 16 h at 55°C with [35S]- and [33P]-labeled (107 c.p.m./mL) single-stranded antisense probes. Following
744 hybridization, sections were treated with 4 µg/mL of RNAse A at 37°C for 1 h, washed with 1X saline-
745 sodium citrate and 50% formamide for 1 h at 55°C, and then with 0.1X saline-sodium citrate at 68°C for 1
746 h. To visualize FG(+) cells, sections were rinsed with PBS and incubated for 1 h at RT in avidin-
747 biotinylated horseradish peroxidase (1:100, ABC kit; Vector Laboratories). Sections were then rinsed, and
748 the peroxidase reaction was developed with 0.05% 3,3'-diaminobenzidine tetrahydrochloride (DAB) and
749 0.003% H_2O_2. Sections were then photographed under bright field illumination and mounted on coated
750 slides. Finally, slides were dipped in Ilford K.5 nuclear tract emulsion (Polysciences; 1:1 dilution in
751 double-distilled water) and exposed in the dark at 4°C for 3-4 weeks before development and photographs
752 of silver-grain epiluminescence.

753 *Data analysis of in situ hybridization studies.* Methods for analysis of *in situ* hybridization material have
754 been described previously[51]. Briefly, pictures were adjusted to match contrast and brightness by using
755 Adobe Photoshop (Adobe Systems). Cell counting was completed independently by three scorers blind to
756 the hypothesis of the study. Radioactive *in situ* material was analyzed using epiluminescence to increase
757 the contrast of silver grains as described previously[65]. FG(+) cells (detected by fluorescence and brown
758 DAB-label) were evaluated for the presence of MOR mRNA: a cell was considered to express MOR
759 mRNA when its soma contained concentric aggregates of silver grains that exceeded background levels.

760 ***Fiber photometry***

761 *Surgery.* Male and female VGluT2::Cre mice (20-30 g; 6-12 weeks) were anesthetized with 1-5%
762 isoflurane and secured to a stereotaxic frame. Using a Micro4 controller and UltraMicroPump, 0.2 µL of a
763 retrograde, Cre-dependent HSV encoding GCaMP6m (HSV-hEF1α-LS1L-GCaMP6m) was injected into

764 the LHb (-1.5 mm AP, +0.45 mm ML, -3.0 mm DV). Syringes were left in place for 7-10 min following
765 injections to minimize diffusion. For fiber photometry calcium imaging experiments, a 400 µm core optic
766 fiber (Doric Lenses) embedded in a 2.5 mm ferrule was implanted over the LPO (+0.5 mm AP, +0.8 mm
767 ML, -5.05 mm DV) and secured to the skull using #000 screws (Fasteners and Metal products Corp;
768 #000-120 X 1/16) and dental cement. Following surgery, mice recovered on a warm heating pad before
769 being transferred back to the vivarium home cage. Three weeks after the virus and fiber surgery, mice
770 were given either SNI or sham control surgery as described above.

771 *Recording.* Signals from GCaMP6 were recorded across 10 trials of stimulation in the Hargreaves test
772 using a Plantar Test Instrument. The onset and offset time for each trial was digitized and sent to an
773 RZ5D (Tucker Davis Technologies). For the acquisition of LPO→LHB activity, GCaMP6 was excited at
774 two wavelengths (490nm, calcium-dependent signal and 405 nm isosbestic control) by amplitude
775 modulated signals from two light-emitting diodes reflected off dichroic mirrors and coupled into a 400µm
776 0.48NA optic fiber. Signals emitted from GCaMP6m and its isosbestic control channel then returned
777 through the same optic fiber and were acquired using photoreceiver (Doric Lenses), digitized at 1kHz,
778 and then recorded by a real-time signal processor (RZ5D; Tucker Davis Technologies) running the
779 Synapse software suite. Analysis of the resulting signal was then performed using custom-written
780 MATLAB scripts available in a general release form at
781 https://github.com/djamesbarker/FiberPhotometry. Briefly, changes in fluorescence across the
782 experimental session (ΔF/F) were calculated by smoothing signals from the isosbestic control channel,
783 scaling the isosbestic control signal by regressing it on the smoothed GCaMP signal, and then generating
784 a predicted 405 nm signal using the linear model generated during the regression. Calcium independent
785 signals on the predicted 405 nm channel were then subtracted from the raw GCaMP signal to remove
786 movement, photo-bleaching, and fiber bending artifacts. Signals from the GCaMP channel were then
787 divided by the control signal to generate the ΔF/F. Peri-event histograms were then created by averaging
788 changes in fluorescence (ΔF/F) across repeated trials during windows encompassing behavioral events of

789 interest. The area under the curve (AUC) was calculated for a pre-stimulation 5 s baseline commencing -
790 10 s before paw withdrawal and for the 5 s period initiated with paw withdrawal.

791 ***Anterograde tracing from the ACC***

792 In rats, unilateral injections of AAV2-hSyn-hChR2(H134R)-mCherry (759 nL) were made throughout
793 anteroposterior range of the ACC (+2.6 to -0.4 mm AP, -0.4 to -0.5 mm ML, -2.6 to -2.8 mm DV). Rats
794 were perfused and brains fixed five weeks later, as described above. Coronal sections (50 µm) containing
795 the ACC and the LHb were collected. After verification of the injection site, every sixth slice containing
796 the LHb was rinsed twice with PBS. Tissue was pre-permeabilized in 1:1 EtOH:PBS for 30 min at 4°C,
797 rinsed briefly in PBS before blocked in 3% H_2O_2 for 10 min. Following PBS washes (3x5 min), tissue
798 was blocked in solution containing normal goat serum (NGS, 10%) for 1 h at RT. Slices were incubated
799 in rabbit anti-mCherry antibody (1:5000 in PBS + 0.3% Triton X100 + NGS 10%; Abcam) overnight at
800 4°C. After PBS washes (4x10 min), slices were incubated in biotinylated goat anti-rabbit secondary
801 antibody (1:200 in PBS; Vector Laboratories) for 2 h at 4°C. Following PBS wash (4x10 min), slices
802 were incubated in VECTASTAIN® ABC Reagent (VECTASTAIN® ABC Kit, Vector Laboratories) for
803 30 min followed by peroxidase substrate (DAB Substrate Kit, Vector Laboratories) for 10 min. Once dark
804 brown DAB precipitate formed, slices were rinsed in PBS (5x5 min), mounted on glass slides, and cover
805 slipped with DEPEX (Electron Microscopy Sciences). DAB-stained fibers were visualized under
806 brightfield illumination and quantified in Stereo Investigator software (MBF Bioscience) using the virtual
807 isotropic space balls probe[66].

808 ***General experimental design***

809 For behavioral experiments, subject numbers were determined by pilot studies and power analyses (power
810 = 0.80, significance level = 0.05, effect size = 15-30%). All behavioral experiments were performed
811 blinded to experimental condition. For immunohistological experiments, three animals with injections

812 targeted at the anterior, middle, and posterior ACC were used to obtain a comprehensive estimation of
813 fibers projecting to the LHb. Electrophysiology experiments were conducted blind to injection site.

814 ***Quantification and statistical analysis***

815 Data are expressed as mean ± SEM or mean with 25th and 75th percentiles as indicated in figure legends
816 and text. Significance was set at $p < 0.05$. Datasets were evaluated to determine whether parametric or
817 non-parametric statistical approaches were most appropriate as indicated in Supplemental Table 1. All
818 tests were two tailed, and statistical analyses were performed in GraphPad Prism or R. The bandwidth for
819 violin plots was determined by Silverman's rule of thumb in Plotly for Python. Sample sizes are reported
820 in figure panels, legends, and Supplementary Table 1. Outliers, including extreme outliers, are reported in
821 Supplementary Table 1 and were not removed from datasets.

822

823 **Reporting summary**

824 Further information on research design is available in the Nature Research Reporting Summary linked to
825 this paper.

826

827 **Data availability**

828 All data described in the main text or extended data are available on Open Science Framework:
829 https://osf.io/mwyb3/?view_only=28fcc13c3cac41a7a55e27ffccd62bda.

830

831 **Authors Contributions**

832 EBM conceived and supervised research. EBM, MWW, and DJB designed the experiments. MWW,
833 KAM, JRD, KAM, and TJC conducted the rat behavioral experiments and LHb innervation mapping.
834 EBM, MWW, KAM, TJC, and KAM performed the rat behavior data analysis. EBM conducted the
835 electrophysiology experiments and data analysis. MM supervised the MOR in situ hybridization study
836 and analysis performed by DJB. CO, SB and DJB conducted the VGluT2::Cre mouse fiber photometry
837 experiments and subsequent data analysis. MWW, KAM, and EBM wrote manuscript with contributions
838 from TJC and DJB. All authors read and approved the final version of the manuscript.

839

840 **Acknowledgements**

841 The authors would like to thank Ryan Carothers, Gabrielle Mintz, Lucy He, Venkateswaran Ganesh, and
842 Benjamin Snyder for their technical assistance with histology, stereotaxic surgeries, and behavioral
843 studies. We also thank Allan Basbaum for feedback on the manuscript. This work was supported by
844 National Institutes of Health grants R01DA042025 (to E.B.M.), K08 NS097632 (to M.W.W.), the
845 Intramural Research Program (IRP) of the National Institute on Drug Abuse (IRP/NIDA/NIH), and a
846 NIDA K99/R00 pathway to independence award (DA043572) to D.J.B.

847

848 **Competing Interests Statement**

849 The authors have no competing interests.

850

851 **Figure Legends**

852 **Figure 1.** *MOR activation in the LHb relieves allodynia and generates negative reinforcement in rats*
853 *with neuropathic pain.* **a,** Timeline of behavioral experiments. Right inset, example injection site centered

854 in LHb. Scale bar = 500 μm. **b,** (Left) Violin plots of 50% mechanical withdrawal thresholds following
855 saline or 10 μM DAMGO microinjections into the LHb in sham males (n = 8) and SNI males (n = 8).
856 Assumption testing for statistical analysis is described in Supplemental Table 1. Sham males: Wilcoxon
857 signed rank test, V = 1.5, p =1. SNI males: Wilcoxon signed rank test, V = 2, p = 0.050. (Right) 50%
858 mechanical withdrawal thresholds following saline or 10 μM DAMGO microinjections into the 3rd
859 ventricle (i.c.v.), in male rats with SNI (n = 12) or sham (n = 9) injuries. Sham: Wilcoxon signed rank
860 test, V = 7, p = 0.53. SNI: Wilcoxon signed rank test, V = 31, p = 0.080. **c**, (Left) 50% mechanical
861 withdrawal thresholds following saline or 10 μM DAMGO microinjections into the LHb of sham females
862 (n = 9) or SNI females (n = 9). Bonferroni corrected paired t test, p = 0.703. Wilcoxon signed rank test, V
863 = 7, p = 0.074. (Right) 50% mechanical withdrawal thresholds following saline or 100 μM DAMGO
864 microinjections into the LHb of sham females (n = 6) or SNI females (n = 8). Sham: Wilcoxon signed
865 rank test, V = 5, p = 1. SNI: Wilcoxon signed rank test, V = 6, p = 0.40. **d**, Difference scores in sham
866 males (n = 8) or SNI males (n = 6) before and after conditioning with intra-LHb microinjections of 10 μM
867 DAMGO vs saline. Two-way mixed ANOVA, significant interaction between SNI/sham and baseline/test
868 F(1,13) = 15.93, p = 0.002; post hoc effect group on test day adjusted p = 0.01; paired t-tests, sham
869 adjusted p = 1; SNI adjusted p = 0.016. (Right) Difference scores in sham males (n = 9) or SNI males (n =
870 12) before and after conditioning with intra-i.c.v. microinjections of 10 μM DAMGO vs saline: Two-way
871 mixed ANOVA, F(1,19) = 2.239, p = 0.15. **e,** (Left) Difference scores in sham females (n = 9) and SNI
872 females (n = 9) before and after conditioning with intra-LHb injections of 10 μM DAMGO vs saline.
873 Sham: Bonferroni corrected t-test p = 0.703. SNI: Wilcoxon signed rank test, V = 7, p = 0.07. (Right)
874 Difference scores in sham females (n = 6) and SNI females (n = 9) before and after conditioning with
875 intra-LHb injections of 100 μM DAMGO vs saline. Two-way mixed ANOVA, significant interaction
876 between SNI/sham and baseline/test F(1,13) = 6.234, p = 0.027; post hoc effect group on test day adjusted
877 p = 0.07; paired t-tests, sham adjusted p = 0.48; SNI adjusted p = 0.035. Means represented by horizontal
878 lines. *p ≤ 0.05, **p ≤ 0.01

879

880 **Figure 2.** *Ongoing pain does not alter MOR agonist synaptic effects or probability of glutamate release*
881 *in the LHb.* Responses to the MOR agonist DAMGO were recorded in voltage clamp, V_m = -60 mV. **a**, In
882 animals with SNI, a subset of neurons responded to bath application of the MOR agonist DAMGO (500
883 nM) with a time locked outward current that was reversed with the MOR selective antagonist CTAP (500
884 nM). Line indicates mean, shading indicates SEM. **b**, Postsynaptic holding current changes in response to
885 bath application of DAMGO were not different between neurons from naïve and SNI rats: Unpaired t-test
886 df = 29, t = 0.87, p = 0.39. Filled circles indicate cells statistically determined to be "responsive" to
887 DAMGO with within cell unpaired t tests. Grey bars indicate 25th and 75th percentiles. **c**, In rats with SNI,
888 DAMGO (500 nM) induced a time locked inhibition of electrically evoked glutamatergic EPSCs, and
889 CTAP (500 nM) partially reversed the effect. Mean ± SEM. **d**, This DAMGO inhibition of electrically
890 evoked EPSC amplitude was not different between LHb neurons from naïve and SNI rats: Unpaired t-test
891 df = 23, t = 0.47, p = 0.64. Baseline probability of release at glutamatergic synapses was similar between
892 LHb neurons in naïve and SNI rats as measured by (**e**) paired pulse ratio (P2/P1) of electrically stimulated
893 EPSCs (50 ms interstimulus interval): Unpaired t-test, df = 24, t = 0.102, p = 0.92; (**f**) baseline
894 spontaneous EPSC frequency: Unpaired t-test unequal variances, df = 37, t = -0.17, p = 0.87; and (**g**)
895 spontaneous EPSC amplitude: Unpaired t-test unequal variances, df = 38, t = -0.09, p = 0.93. Data from
896 naïve rats previously published in[18].

897

898 **Figure 3.** *Glutamatergic inputs to the LHb from the LPO are inhibited by MOR activation.* **a,** Schematic
899 diagram of AAV2-hSyn-hChR2(H134R)-mCherry injection targets which project to the LHb. **b**,
900 Proportions of LHb neurons receiving functional synaptic connections from six input regions measured
901 with optogenetic stimulation of terminals expressing ChR2. **c**, Among connected neurons, venn diagrams
902 depict the numbers of LHb cells receiving optically stimulated glutamatergic and/or GABAergic synaptic

903 input. **d,** (Left) Experiment design: DAMGO (500 nM) was applied during optical synaptic stimulation
904 experiments to probe for functional MOR presynaptic control of glutamate release from specific inputs.
905 (Right) Change from baseline amplitude of optically-evoked EPSCs during DAMGO application. EPSCs
906 from LPO terminal stimulation were most strongly inhibited by MOR activation: One-way ANOVA, df =
907 4, F = 4.11, p = 0.0057 followed by Tukey HSD pairwise comparisons. **e**, (Left) Representative traces of
908 optically-evoked EPSCs in an LHb neuron from a rat with ChR2 expressed in inputs from the LPO.
909 DAMGO decreased the amplitude of light-evoked EPSC, which was partially reversed by the selective
910 MOR antagonist CTAP (500 nM). Rise time was < 2 ms, indicative of a monosynaptic response. (Right)
911 Summary time course of the DAMGO inhibition across all optically-evoked LPO-LHb EPSCs (n = 12).
912 **f,** LPO inputs to the LHb in female rats (left) had a similar overall connectivity rate but (middle) more
913 GABAergic connections than glutamate connections. (Right) DAMGO inhibited light-evoked
914 glutamatergic synaptic inputs from the LPO to the LHb in female rats as well. *p < 0.05, **p < 0.01

915

916 **Figure 4.** *LPO inputs to the LHb highly express MOR mRNA.* **a,** Schematic of unilateral iontophoretic
917 deposition of the retrograde tracer FG into the LHb. **b**, FG injection sites in LHb (n = 3 rats). **c,** (Left and
918 middle) Representative brightfield images of FG-positive/MOR-positive somas (yellow arrowhead) and
919 FG-positive/MOR-negative somas (blue arrowhead) in the LPO. Scale bar = 20 µm. (Right) Darkfield
920 image of in situ hybridization localization for MOR mRNA (OPRM1). **d,** Number of MOR-positive/FG-
921 positive (yellow) and MOR-negative/FG-positive (blue) cells in various basal forebrain regions. **e**, Donut
922 plot depicting proportions of total MOR-positive inputs to the LHb from various basal forebrain regions.
923 **f,** Locations of FG-positive/MOR-positive (red) and FG-positive/MOR-negative (blue) somata throughout
924 basal forebrain. Co-labeled cells are separated from the singly labelled population for display purposes.

925

926 **Figure 5.** *LHb MOR activation relieves aversiveness of glutamatergic LPO input to the LHb*. **a,**
927 Schematic diagram of dual virus injections to express ChR2-mCherry or mCherry selectively in LPO
928 neurons that project to the LHb, and optic fiber implantation targeting the LPO cell bodies in male rats. **b**,
929 Representative images of Cre-dependent ChR2-mCherry fluorescence in LPO cell bodies. (Left) Scale bar
930 = 250 µm. (Right) Lesion from optic fiber ("o.f.") implant amidst ChR2-mCherry-expressing cell bodies.
931 Scale bar = 50 µm. **c,** Bilateral activation of the LPO-LHb projection in rats (n = 8) produced a robust
932 conditioned place aversion to the stimulation paired side of the place conditioning apparatus (paired t-test,
933 df = 7, t = -4.64, p = 0.002)**. d,** Rats received bilateral blue light stimulation in both conditioning
934 chambers, concomitant with intra-LHb DAMGO in one conditioning chamber or intra-LHb saline in the
935 other. Only animals with active ChR2 (n = 8), but not mCherry controls (n = 8), developed a preference
936 for the intra-LHb DAMGO paired side of the place conditioning apparatus. Two-way mixed ANOVA,
937 significant interaction between ChR2-mCherry/mCherry and baseline/test F(1,14) = 9.982, p = 0.007;
938 post hoc effect group on test day adjusted p = 0.006; paired t-tests, mCherry adjusted p = 0.427; ChR2-
939 mCherry adjusted p = 0.0027. **e**, Schematic diagram of dual virus injections to express iC++-eYFP
940 selectively in LPO neurons that project to the LHb, and optic fiber implantation targeting the LPO cell
941 bodies in male rats that underwent either sham or spared nerve injury. **f**, Representative image of cre-
942 dependent iC++-eYFP fluorescence in LPO cell bodies. Scale bar = 50 µm. **g,** Representative cell-
943 attached recording in current clamp mode of an LPO neurons expressing iC++-eYFP fluorescence, where
944 blue light stimulation paused neuronal firing. **h,** (Left) Rats which had undergone either sham or spared
945 nerve injury two weeks before received bilateral blue light induced inhibition in one chamber or no light
946 in another chamber. (Right) Only animals with spared nerve injury (n = 7), but not sham injury (n = 5)
947 developed a preference for the blue light paired side of the place conditioning apparatus. Two-way mixed
948 ANOVA, trending interaction between sham/spared nerve injury (SNI) and baseline/test F(1,10) = 3.443,
949 p = 0.093; post hoc paired t-tests for sham adjusted p = 0.580; spared nerve injury (SNI) adjusted p =
950 0.048. **i,** Schematic diagram of HSV-hEF1α-LS1L-GCaMP6m injection into the LHb of VGluT2::Cre

951 mice, to induce expression of GCaMP6m in glutamatergic LPO neurons innervating the LHb, and optic
952 fiber implant for fiber photometry imaging in the LHb-projecting LPO neurons. (Right) Experimental
953 timeline. **j**, Mice with SNI (green, n = 5) exhibited significantly larger changes in GCaMP6m
954 fluorescence time-locked to paw withdrawal in response to thermal stimulation in the Hargreaves
955 apparatus compared to sham controls (grey, n = 9): Two-way ANOVA, $F(1,12) = 5.439$, $p = 0.038$;
956 Holm-Sidak post-hoc test, $p = 0.0074$. *$p < 0.05$, **$p < 0.01$, ***$p < 0.005$

957

958 **Figure 6.** Summary: LHb-projecting LPO glutamatergic neurons that fire more during pain provide an
959 aversive signal. MOR activation in the LHb inhibits the glutamate release from the LPO, preventing
960 propagation of the aversive signal further in the circuit.

961

962 **Extended Data Figure Legends**

963 **Extended Data Figure 1.** *Further characterization of neuropathic pain and inflammatory pain models*
964 *and the impact of intra-LHb MOR activation in rat.* **a,** (Left) Violin plots of withdrawal latency to heat in
965 male sham (n = 9) and SNI (n = 8) rats with SNI after saline vs DAMGO (10 μM) microinjections into
966 the LHb. Two-way mixed ANOVA revealed no significant interaction between injury and drug condition
967 ($F(1,14) = 2.522$, $p = 0.135$) in the intra-LHb male cohort (Left). Bonferroni corrected paired t test was
968 conducted between drug conditions for normally distributed Sham (Sham males: $p = .861$) and SNI (SNI
969 males: $p = 0.096$) animals. Two-way mixed ANOVA indicated no significant interaction between injury
970 and drug condition ($F(1,19) = 1.549$, $p = 0.228$) in male intra-i.c.v. cohort (Right). Sham animals were
971 non-parametrically distributed, the Wilcoxon signed rank test was conducted ($V = 24$, $p = 0.9102$) while
972 SNI animals were normally distributed, and a Bonferroni corrected paired t test was conducted ($p =$
973 0.0433). **b,** Two-way mixed ANOVA indicated no significant interaction between injury and drug
974 condition ($F(1,16) = 0.008$, $p = 0.929$). Both the Sham and SNI female groups were non-parametrically

975 distributed, the Wilcoxon signed rank test was conducted, both conditions yielding non-significant
976 differences (V = 13, p = 0.3008). **c,** To test if the effects of MOR activation in the LHb generalize to
977 other forms of pain, we repeated the manipulations above with an inflammatory model of pain. Male rats
978 received an intradermal injection of CFA or sterile saline into the plantar aspect of the hindpaw.
979 Schematic diagram of inflammatory injury preparations and cannulation targeting the LHb. **d**,
980 Mechanical withdrawal thresholds in sham and CFA-injured rats. In animals with CFA, we observed an
981 increase in the average withdrawal threshold following intra-LHb DAMGO (10 μM) compared to saline,
982 indicating a reduction in mechanical allodynia: Two-way mixed ANOVA revealed significant injury and
983 drug condition interaction (F(1,13) = 5.772, p = 0.032) with Bonferroni corrected paired t-test, SNI p =
984 0.0178; saline p = 0.796. **e**, Withdrawal latency to heat. DAMGO in the LHb did not reverse the CFA-
985 induced decrease in withdrawal latency to heat. Two-way mixed ANOVA revealed no significant injury
986 and drug condition interaction (F(1,13) = 2.589, p = 0.132). Bonferroni corrected pair t tests were
987 conducted; saline: p = 0.455; CFA: Wilcoxon signed rank test, V = 33, p = 0.25. **f**, Rats with CFA injury
988 also did not develop a preference to intra-LHb DAMGO in the place conditioning paradigm: Two-way
989 mixed ANOVA, no significant interaction between CFA/saline and baseline/test F (1,11) = 0.104, p =
990 0.753. Bonferroni corrected t tests were conducted between drug conditions for saline (saline: p = 0.901)
991 or CFA (CFA: p = 0.706) treated animals. The discrepancy between place conditioning results of our
992 neuropathic and inflammatory pain animals may be due to the natural history of the injury caused in the
993 CFA model: whereas SNI animals underwent permanent nerve ligation, animals injected with CFA
994 presented with transient swelling and erythema of the hindpaw. Within a few days of CFA injection, this
995 phenotype had resolved in our rats. **g,** Mechanical allodynia also reversed quickly: in a separate cohort of
996 rats, all subjects displayed a sharp decline in withdrawal threshold from baseline on day 1 following CFA
997 injection, but the injury-induced allodynia returned to control levels by day 5 in many animals. Individual
998 animals were tested daily; each line represents a male rat. **h,** Average across rats shows that our CFA-
999 induced reduction in mechanical allodynia reversed within a few days. Since our place conditioning

1000 training exceeds this time window, resolution of the injury probably occurred before training was
1001 completed, thus preventing the formation of a robust association between pain relief and place
1002 conditioning apparatus context to produce a CPP. Circles or squares indicate individual animals, while
1003 connecting lines indicate within-subject manipulations. *$p \leq 0.05$

1004

1005 **Extended Data Figure 2.** *Neurons receiving functional synaptic inputs from the five brain regions*
1006 *showing connectivity were distributed throughout the LHb.* Locations of neurons with functional synaptic
1007 connections detected using whole-cell recordings from optogenetic stimulation of terminals arising from
1008 each input tested. Locations are based on a combination of biocytin immunohistochemistry localization
1009 and low magnification visualization of the cell location during recording. Color indicates source of
1010 innervation.

1011

1012 **Extended Data Figure 3.** *ACC minimally innervates the LHb.* **a**, Diagram of the extent of unilateral
1013 AAV2-hSyn-hChR2(H134R)-mCherry injection sites (n = 9 male rats) throughout anteroposterior range
1014 of the ACC for anterograde tracing study. **b,** Example ipsilateral DAB-positive fibers (black) visualized
1015 under brightfield illumination. Fibers heavily innervate the MDL, which abuts the lateral edge of the LHb,
1016 while sparse to no fibers innervate the LHb. Contralateral innervation of LHb and MDL was negligible
1017 compared to the ipsilateral side, and therefore were omitted from our analysis. (Left) Scale bar = 250 µm.
1018 (Right) Scale bar = 50 µm. **c**, Average stereologically-quantified DAB-positive fiber lengths throughout
1019 anteroposterior range of the LHb, compared to the MDL innervation in the same coronal slice. Mann-
1020 Whitney test, two-tailed: $U = 0$, $p = 0.0006$.

1021

1022 **Extended Data Figure 4.** *Sources of glutamatergic inputs to the rat LHb vary in strength and delay in*
1023 *synaptic transmission.* **a**, We observed some variations between inputs in the mean light evoked EPSCs

1024 (V_m = -60 mV). In particular, excitatory inputs from the VTA were consistently small: Kruskal-Wallis $\chi 2$
1025 = 25.5, df = 4, p = 0.00004, followed by Dunn Test for pairwise comparisons. **b**, Differences were also
1026 detected in the delay to the onset of light evoked EPSCs to LHb neurons from these different sources,
1027 with inputs from LH showing the fastest response. Although these data deviate from a normal
1028 distribution (Shapiro's test, p = 0.0000001), KDEs (violins) are consistent with continuous distributions,
1029 suggesting reliable polysynaptic events were rarely detected. **c**, We observed some variations between
1030 inputs in the mean light evoked IPSCs (V_m = -40 mV). While there were no statistically significant
1031 differences in amplitudes detected, the mean inhibitory input from the VP was particularly small:
1032 Kruskal-Wallis $\chi 2$ = 2.3, df = 4, p = 0.7. ** $p < 0.01$, *** $p < 0.005$, **** $p < 0.0005$

1033

1034 **Extended Data Figure 5.** *Optogenetic experiments detect local glutamate, but not GABA, functional*
1035 *connections in rat LHb.* AAV2-hSyn-hChR2(H134R)-mCherry was stereotaxically injected into the LHb
1036 at least 4 weeks prior to *ex vivo* whole cell recordings in the LHb to detect local synaptic connections.
1037 Neurons were recorded blind to ChR2 expression, therefore in some cases the patched neuron expressed
1038 ChR2. Therefore, in addition to connectivity criteria used for other afferent inputs, in these experiments
1039 only light evoked inward currents that were blocked by 10 μM DNQX were considered glutamatergic
1040 connections, and direct ChR2 induced inward currents were subtracted out for the quantification
1041 illustrated here. Each cell was probed for both glutamate and GABA inputs in voltage clamp by holding
1042 neurons at V_m = -60 mV and -40 mV, light pulse durations 1, 5, and 10 ms durations. **a**, Example
1043 recording at V_m = -60 mV showing a light evoked response that was blocked by DNQX. **b**, Example
1044 recording at V_m = -40 mV with minimal outward current response within 7 ms of light pulse. This
1045 example is the largest outward deflection from baseline observed in these experiments. **c**, Summary of all
1046 LHb recordings tested in this experiment. Filled circles represent cells where responses could be
1047 classified as local ChR2 induced synaptic transmission. When no clear response was detected, the
1048 measure indicated is the difference between the mean $I_{holding}$ of the baseline 100 ms period just prior to the

1049 light pulse and the mean $I_{holding}$ 2 ms period starting 2 ms after initiation of the light pulse, consistent with
1050 monosynaptic delay timing. None of the recordings made at V_m = -40 mV met the criteria for a response
1051 to light stimulation with an outward current.

1052

1053 **Extended Data Figure 6.** *Isolated monosynaptic glutamatergic inputs from LPO to LHb neurons are*
1054 *inhibited by MOR activation.* **a,** Example light evoked EPSC responses in an LHb neuron from a rat with
1055 ChR2 expression in LPO neurons. This response persisted in monosynaptic isolation by 500 nM TTX and
1056 100 μM 4 AP (green), and this isolated response was inhibited by 500 nM DAMGO (magenta). **b**,
1057 Summary of DAMGO effects on isolated monosynaptic EPSC inputs to LHb neurons expressed as % of
1058 baseline monosynaptic response (left) and as raw EPSC magnitudes (right). Paired t-test, df = 4, t = -5.1,
1059 p = 0.007. ** p < 0.01

1060

1061 **Extended Data Figure 7.** *Mice with SNI show hypersensitivity to heat and increased activity in LHb-*
1062 *projecting LPO neurons during paw withdrawal from thermal stimulation.* **a,** Mice with SNI show a
1063 reduced latency to withdraw their paw following thermal stimulation in the Hargreaves task. Unpaired t-
1064 test, t(12) = 3.007, p = 0.011. **b,** VGluT2-expressing LPO neurons that project to the LHb expressed
1065 GCaMP6m and showed a greater calcium response during paw withdrawal to Hargreaves thermal
1066 stimulation (area under the curve, deviation from baseline fluorescence) in SNI animals (n = 5) compared
1067 to sham controls (n = 9): Two-way ANOVA, F(1,12) = 5.4, p = 0.038; Holm-Sidak post-hoc test, p =
1068 0.0074. ** p < 0.01

1069

1070 **Extended Data Figure 8.** Locations and spread of bilateral ChR2 (a) and iC++ (b) expression in the
1071 LPO in rats used for *in vivo* optogenetic experiments in Fig 5.

1072

1073 **References**

1074 1. Matsumoto, M. & Hikosaka, O. Representation of negative motivational value in the primate lateral
1075 habenula. *Nat Neurosci* **12**, 77–84 (2009).
1076 2. Benabid, A. L. & Jeaugey, L. Cells of the rat lateral habenula respond to high-threshold
1077 somatosensory inputs. *Neurosci Lett* **96**, 289–94 (1989).
1078 3. Dafny, N. & Qiao, J. T. Habenular neuron responses to noxious input are modified by dorsal raphe
1079 stimulation. *Neurol. Res.* **12**, 117–121 (1990).
1080 4. Nagao, M., Kamo, H., Akiguchi, I. & Kimura, J. Induction of c-Fos-like protein in the lateral habenular
1081 nucleus by persistent noxious peripheral stimulation. *Neurosci. Lett.* **151**, 37–40 (1993).
1082 5. Huang, T. *et al.* Identifying the pathways required for coping behaviours associated with sustained
1083 pain. *Nature* **565**, 86–90 (2019).
1084 6. Matsumoto, M. & Hikosaka, O. Lateral habenula as a source of negative reward signals in dopamine
1085 neurons. *Nature* **447**, 1111–1115 (2007).
1086 7. Li, B. *et al.* Synaptic potentiation onto habenula neurons in the learned helplessness model of
1087 depression. *Nature* **470**, 535–539 (2011).
1088 8. Poller, W. C., Madai, V. I., Bernard, R., Laube, G. & Veh, R. W. A glutamatergic projection from the
1089 lateral hypothalamus targets VTA-projecting neurons in the lateral habenula of the rat. *Brain Res*
1090 **1507**, 45–60 (2013).
1091 9. Herkenham, M. & Nauta, W. J. Afferent connections of the habenular nuclei in the rat. A horseradish
1092 peroxidase study, with a note on the fiber-of-passage problem. *J Comp Neurol* **173**, 123–46 (1977).
1093 10. Vertes, R. P. Analysis of projections from the medial prefrontal cortex to the thalamus in the rat,
1094 with emphasis on nucleus reuniens. *J. Comp. Neurol.* **442**, 163–187 (2002).

1095 11. Yetnikoff, L., Cheng, A. Y., Lavezzi, H. N., Parsley, K. P. & Zahm, D. S. Sources of input to the
1096 rostromedial tegmental nucleus, ventral tegmental area, and lateral habenula compared: A study in
1097 rat. *J Comp Neurol* **523**, 2426–56 (2015).
1098 12. Kim, U. & Lee, T. Topography of descending projections from anterior insular and medial prefrontal
1099 regions to the lateral habenula of the epithalamus in the rat. *Eur J Neurosci* **35**, 1253–69 (2012).
1100 13. Araki, M., McGeer, P. L. & Kimura, H. The efferent projections of the rat lateral habenular nucleus
1101 revealed by the PHA-L anterograde tracing method. *Brain Res.* **441**, 319–330 (1988).
1102 14. Quina, L. A. *et al.* Efferent pathways of the mouse lateral habenula. *J Comp Neurol* **523**, 32–60
1103 (2015).
1104 15. Taylor, N. E. *et al.* The rostromedial tegmental nucleus: a key modulator of pain and opioid
1105 analgesia. *Pain* **160**, 2524–2534 (2019).
1106 16. Cohen, S. R. & Melzack, R. Morphine injected into the habenula and dorsal posteromedial thalamus
1107 produces analgesia in the formalin test. *Brain Res.* **359**, 131–139 (1985).
1108 17. Navratilova, E. *et al.* Pain relief produces negative reinforcement through activation of mesolimbic
1109 reward-valuation circuitry. *Proc Natl Acad Sci U A* **109**, 20709–13 (2012).
1110 18. Margolis, E. B. & Fields, H. L. Mu Opioid Receptor Actions in the Lateral Habenula. *PLoS One* **11**,
1111 e0159097 (2016).
1112 19. Decosterd, I. & Woolf, C. J. Spared nerve injury: an animal model of persistent peripheral
1113 neuropathic pain. *PAIN* **87**, 149–158 (2000).
1114 20. Miaskowski, C. *et al.* Does opioid analgesia show a gender preference for females? *Pain Forum* **8**,
1115 34–44 (1999).
1116 21. Kest, B., Sarton, E. & Dahan, A. Gender differences in opioid-mediated analgesia: animal and human
1117 studies. *Anesthesiology* **93**, 539–547 (2000).
1118 22. Kepler, K. L. *et al.* Gender effects and central opioid analgesia. *Pain* **45**, 87–94 (1991).

1119 23. Thompson, S. J. *et al.* Chronic neuropathic pain reduces opioid receptor availability with associated
1120 anhedonia in rat. *Pain* **159**, 1856–1866 (2018).
1121 24. Porreca, F. *et al.* Spinal opioid mu receptor expression in lumbar spinal cord of rats following nerve
1122 injury. *Brain Res.* **795**, 197–203 (1998).
1123 25. Zhang, X. *et al.* Down-regulation of mu-opioid receptors in rat and monkey dorsal root ganglion
1124 neurons and spinal cord after peripheral axotomy. *Neuroscience* **82**, 223–240 (1998).
1125 26. Shabel, S. J., Proulx, C. D., Trias, A., Murphy, R. T. & Malinow, R. Input to the lateral habenula from
1126 the basal ganglia is excitatory, aversive, and suppressed by serotonin. *Neuron* **74**, 475–481 (2012).
1127 27. Lecca, S. *et al.* Aversive stimuli drive hypothalamus-to-habenula excitation to promote escape
1128 behavior. *eLife* **6**, (2017).
1129 28. Hu, H., Cui, Y. & Yang, Y. Circuits and functions of the lateral habenula in health and in disease. *Nat.*
1130 *Rev. Neurosci.* **21**, 277–295 (2020).
1131 29. Root, D. H., Mejias-Aponte, C. A., Qi, J. & Morales, M. Role of glutamatergic projections from ventral
1132 tegmental area to lateral habenula in aversive conditioning. *J Neurosci* **34**, 13906–10 (2014).
1133 30. Barker, D. J. *et al.* Lateral Preoptic Control of the Lateral Habenula through Convergent Glutamate
1134 and GABA Transmission. *Cell Rep.* **21**, 1757–1769 (2017).
1135 31. Fields, H. State-dependent opioid control of pain. *Nat Rev Neurosci* **5**, 565–75 (2004).
1136 32. Tooley, J. *et al.* Glutamatergic Ventral Pallidal Neurons Modulate Activity of the Habenula-
1137 Tegmental Circuitry and Constrain Reward Seeking. *Biol. Psychiatry* **83**, 1012–1023 (2018).
1138 33. Johansen, J. P., Fields, H. L. & Manning, B. H. The affective component of pain in rodents: direct
1139 evidence for a contribution of the anterior cingulate cortex. *Proc. Natl. Acad. Sci. U. S. A.* **98**, 8077–
1140 8082 (2001).
1141 34. LaGraize, S. C., Borzan, J., Peng, Y. B. & Fuchs, P. N. Selective regulation of pain affect following
1142 activation of the opioid anterior cingulate cortex system. *Exp. Neurol.* **197**, 22–30 (2006).

1143 35. Kim, U. & Chang, S. Y. Dendritic morphology, local circuitry, and intrinsic electrophysiology of
1144 neurons in the rat medial and lateral habenular nuclei of the epithalamus. *J Comp Neurol* **483**, 236–
1145 50 (2005).
1146 36. Flanigan, M. E. *et al.* Orexin signaling in GABAergic lateral habenula neurons modulates aggressive
1147 behavior in male mice. *Nat. Neurosci.* **23**, 638–650 (2020).
1148 37. Zhang, L. *et al.* A GABAergic cell type in the lateral habenula links hypothalamic homeostatic and
1149 midbrain motivation circuits with sex steroid signaling. *Transl. Psychiatry* **8**, 50 (2018).
1150 38. Quina, L. A., Walker, A., Morton, G., Han, V. & Turner, E. E. GAD2 Expression Defines a Class of
1151 Excitatory Lateral Habenula Neurons in Mice that Project to the Raphe and Pontine Tegmentum.
1152 *eNeuro* **7**, (2020).
1153 39. Wallace, M. L. *et al.* Anatomical and single-cell transcriptional profiling of the murine habenular
1154 complex. *eLife* **9**, (2020).
1155 40. Mansour, A., Khachaturian, H., Lewis, M. E., Akil, H. & Watson, S. J. Autoradiographic differentiation
1156 of mu, delta, and kappa opioid receptors in the rat forebrain and midbrain. *J. Neurosci. Off. J. Soc.*
1157 *Neurosci.* **7**, 2445–2464 (1987).
1158 41. Kang, S. *et al.* Downregulation of M-channels in lateral habenula mediates hyperalgesia during
1159 alcohol withdrawal in rats. *Sci. Rep.* **9**, 2714 (2019).
1160 42. Li, J., Li, Y., Zhang, B., Shen, X. & Zhao, H. Why depression and pain often coexist and mutually
1161 reinforce: Role of the lateral habenula. *Exp. Neurol.* **284**, 106–113 (2016).
1162 43. Li, Y. *et al.* Role of the Lateral Habenula in Pain-Associated Depression. *Front. Behav. Neurosci.* **11**,
1163 31 (2017).
1164 44. Bernal, S. A., Morgan, M. M. & Craft, R. M. PAG mu opioid receptor activation underlies sex
1165 differences in morphine antinociception. *Behav. Brain Res.* **177**, 126–133 (2007).

1166 45. Mogil, J. S., Chesler, E. J., Wilson, S. G., Juraska, J. M. & Sternberg, W. F. Sex differences in thermal
1167 nociception and morphine antinociception in rodents depend on genotype. *Neurosci. Biobehav. Rev.*
1168 **24**, 375–389 (2000).
1169 46. Weiss, T. & Veh, R. W. Morphological and electrophysiological characteristics of neurons within
1170 identified subnuclei of the lateral habenula in rat brain slices. *Neuroscience* **172**, 74–93 (2011).
1171 47. Metzger, M. *et al.* Habenular connections with the dopaminergic and serotonergic system and their
1172 role in stress-related psychiatric disorders. *Eur. J. Neurosci.* (2019) doi:10.1111/ejn.14647.
1173 48. Meye, F. J. *et al.* Shifted pallidal co-release of GABA and glutamate in habenula drives cocaine
1174 withdrawal and relapse. *Nat. Neurosci.* **19**, 1019–1024 (2016).
1175 49. Shabel, S. J., Proulx, C. D., Piriz, J. & Malinow, R. Mood regulation. GABA/glutamate co-release
1176 controls habenula output and is modified by antidepressant treatment. *Science* **345**, 1494–8 (2014).
1177 50. Langlois, L. D. *et al.* Potentiation of glutamatergic synaptic transmission onto lateral habenula
1178 neurons following early life stress and intravenous morphine self-administration in rats. *Addict. Biol.*
1179 e13064 (2021) doi:10.1111/adb.13064.
1180 51. Root, D. H. *et al.* Selective Brain Distribution and Distinctive Synaptic Architecture of Dual
1181 Glutamatergic-GABAergic Neurons. *Cell Rep.* **23**, 3465–3479 (2018).
1182 52. Newman, H. M., Stevens, R. T. & Apkarian, A. V. Direct spinal projections to limbic and striatal areas:
1183 anterograde transport studies from the upper cervical spinal cord and the cervical enlargement in
1184 squirrel monkey and rat. *J. Comp. Neurol.* **365**, 640–658 (1996).
1185 53. Burstein, R., Cliffer, K. D. & Giesler, G. J. Direct somatosensory projections from the spinal cord to
1186 the hypothalamus and telencephalon. *J. Neurosci. Off. J. Soc. Neurosci.* **7**, 4159–4164 (1987).
1187 54. Hori, T., Oka, T., Hosoi, M. & Aou, S. Pain modulatory actions of cytokines and prostaglandin E2 in
1188 the brain. *Ann. N. Y. Acad. Sci.* **840**, 269–281 (1998).

1189 55. Ono, T. & Nakamura, K. Learning and integration of rewarding and aversive stimuli in the rat lateral
1190 hypothalamus. *Brain Res.* **346**, 368–373 (1985).
1191 56. Almli, C. R. & McMullen, N. T. Ontogeny of lateral preoptic unit activity in rats. *Brain Res. Bull.* **4**,
1192 773–781 (1979).
1193 57. Vowles, K. E. *et al.* Rates of opioid misuse, abuse, and addiction in chronic pain: a systematic review
1194 and data synthesis. *Pain* **156**, 569–576 (2015).
1195 58. Zadina, J. E. *et al.* Endomorphin analog analgesics with reduced abuse liability, respiratory
1196 depression, motor impairment, tolerance, and glial activation relative to morphine.
1197 *Neuropharmacology* **105**, 215–227 (2016).
1198 59. Chakraborty, S. *et al.* A Novel Mitragynine Analog with Low-Efficacy Mu Opioid Receptor Agonism
1199 Displays Antinociception with Attenuated Adverse Effects. *J. Med. Chem.* **64**, 13873–13892 (2021).
1200 60. Ehrlich, A. T. *et al.* Expression map of 78 brain-expressed mouse orphan GPCRs provides a
1201 translational resource for neuropsychiatric research. *Commun. Biol.* **1**, 102 (2018).
1202 61. Wagner, F., Bernard, R., Derst, C., French, L. & Veh, R. W. Microarray analysis of transcripts with
1203 elevated expressions in the rat medial or lateral habenula suggest fast GABAergic excitation in the
1204 medial habenula and habenular involvement in the regulation of feeding and energy balance. *Brain*
1205 *Struct. Funct.* **221**, 4663–4689 (2016).
1206 62. Broms, J. *et al.* Monosynaptic retrograde tracing of neurons expressing the G-protein coupled
1207 receptor Gpr151 in the mouse brain. *J. Comp. Neurol.* **525**, 3227–3250 (2017).
1208 63. Paxinos, G. & Watson, C. *The Rat Brain in Stereotaxic Coordinates, Compact*. (Academic Press, 1997).
1209 64. Chaplan, S. R., Bach, F. W., Pogrel, J. W., Chung, J. M. & Yaksh, T. L. Quantitative assessment of
1210 tactile allodynia in the rat paw. *J. Neurosci. Methods* **53**, 55–63 (1994).
1211 65. Yamaguchi, T., Wang, H.-L., Li, X., Ng, T. H. & Morales, M. Mesocorticolimbic glutamatergic pathway.
1212 *J. Neurosci. Off. J. Soc. Neurosci.* **31**, 8476–8490 (2011).

1213 66. Mouton, P. R., Gokhale, A. M., Ward, N. L. & West, M. J. Stereological length estimation using
1214 spherical probes. *J. Microsc.* **206**, 54–64 (2002).
1215

Figure 1

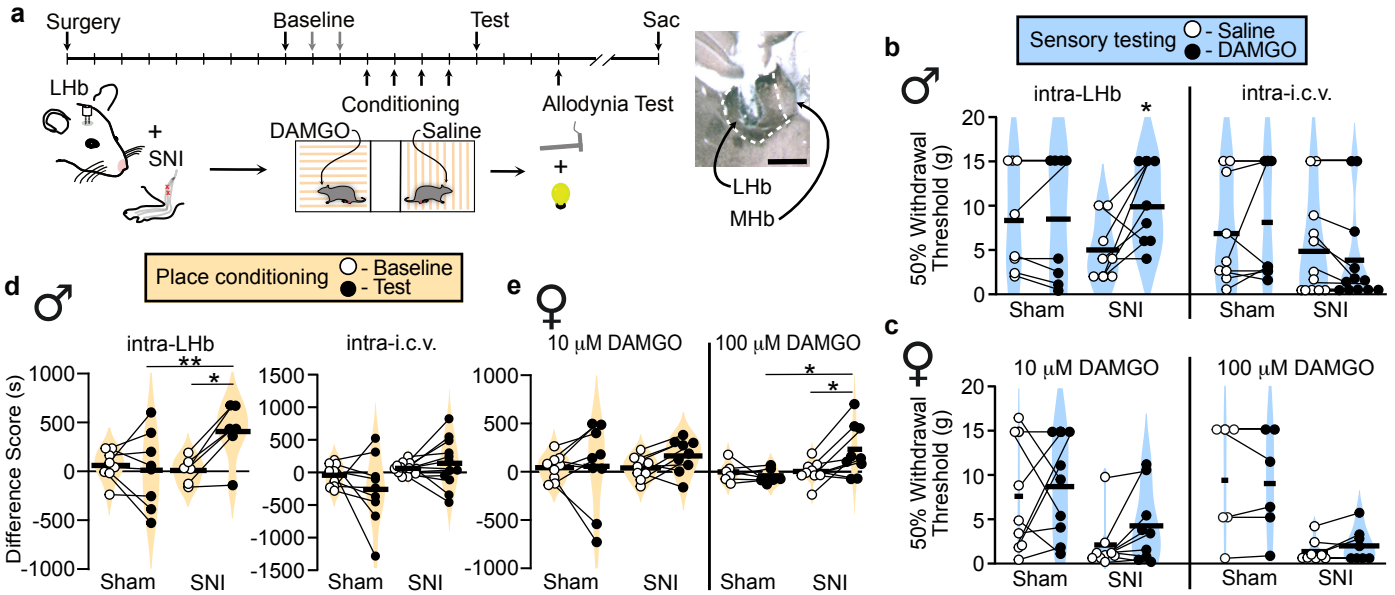
a
Surgery
Baseline
Test
Sac
LHb
+
SNI
Conditioning
DAMGO
Saline
Allodynia Test
+
LHb
MHb
b
Sensory testing
- Saline
- DAMGO
intra-LHb
intra-i.c.v.
50% Withdrawal Threshold (g)
Sham
SNI
c
10 μM DAMGO
100 μM DAMGO
d
Place conditioning
- Baseline
- Test
intra-LHb
intra-i.c.v.
Difference Score (s)
e
10 μM DAMGO
100 μM DAMGO

Figure 2

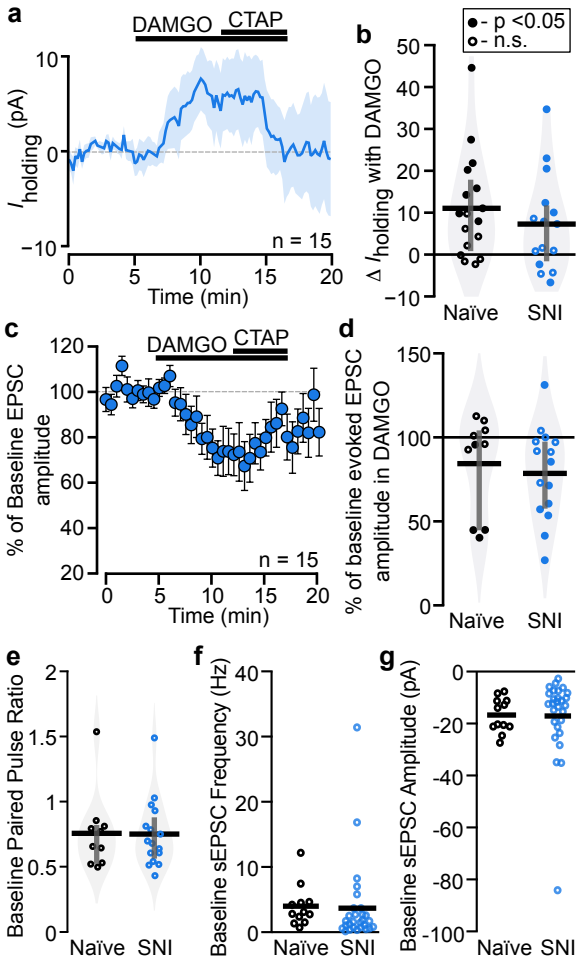
a
DAMGO
CTAP
10
0
−10
$I_{holding}$ (pA)
n = 15
0
5
10
15
20
Time (min)
b
● - p <0.05
○ - n.s.
50
40
30
20
10
0
−10
Δ $I_{holding}$ with DAMGO
Naïve
SNI
c
DAMGO
CTAP
120
100
80
60
40
20
% of Baseline EPSC amplitude
n = 15
0
5
10
15
20
Time (min)
d
150
100
50
0
% of baseline evoked EPSC amplitude in DAMGO
Naïve
SNI
e
2
1.5
1
0.5
0
Baseline Paired Pulse Ratio
Naïve
SNI
f
40
30
20
10
0
Baseline sEPSC Frequency (Hz)
Naïve
SNI
g
0
-20
-40
-60
-80
-100
Baseline sEPSC Amplitude (pA)
Naïve
SNI

Figure 3

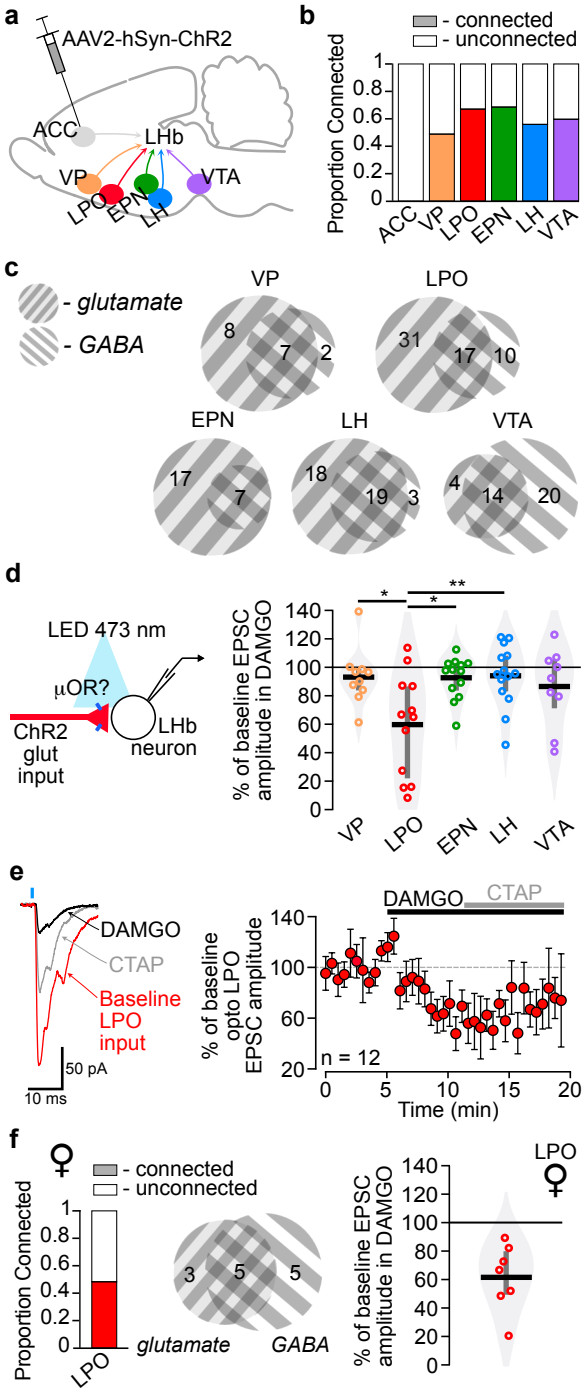
a
AAV2-hSyn-ChR2
ACC
LHb
VP
VTA
LPO
EPN
LH
b
- connected
- unconnected
Proportion Connected
ACC
VP
LPO
EPN
LH
VTA
c
- glutamate
- GABA
VP
LPO
EPN
LH
VTA
d
LED 473 nm
μOR?
ChR2
glut
input
LHb
neuron
% of baseline EPSC
amplitude in DAMGO
VP
LPO
EPN
LH
VTA
e
DAMGO
CTAP
Baseline
LPO
input
50 pA
10 ms
% of baseline
opto LPO
EPSC amplitude
n = 12
Time (min)
f
- connected
- unconnected
Proportion Connected
LPO
glutamate
GABA
% of baseline EPSC
amplitude in DAMGO

Figure 4

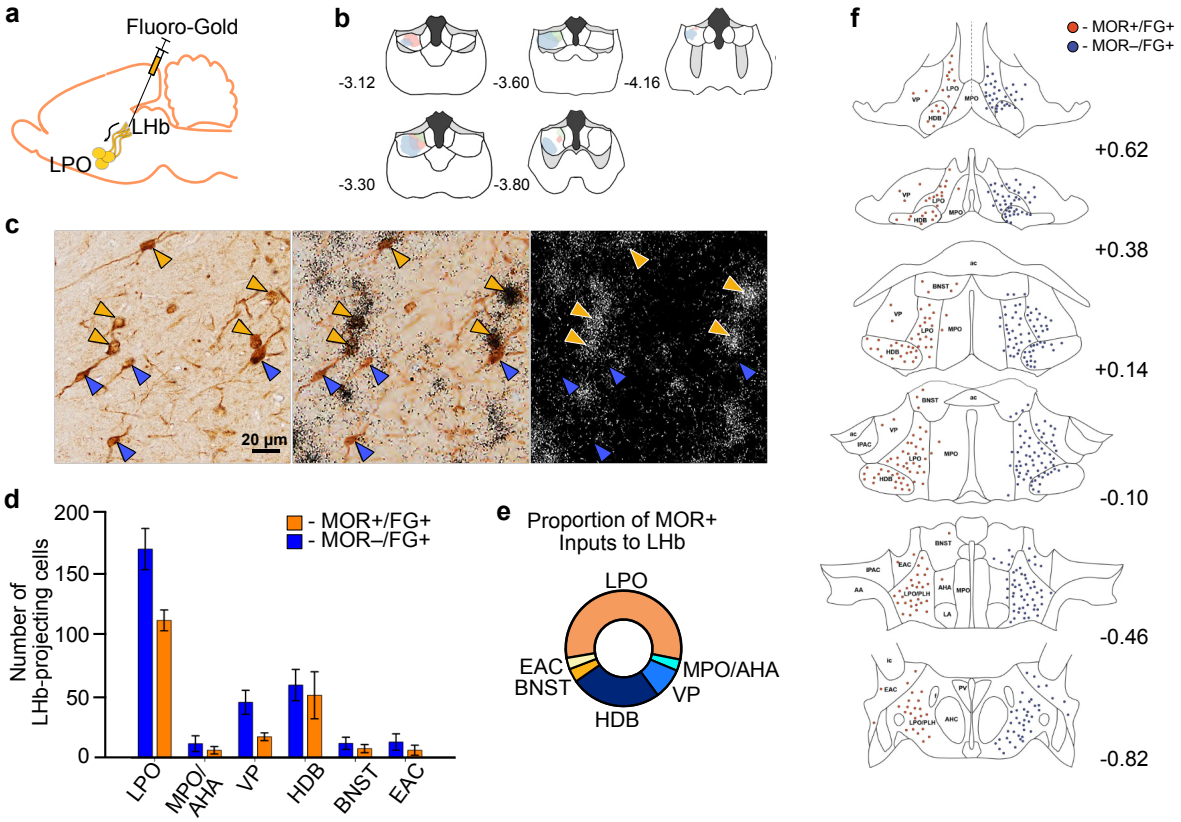
a
Fluoro-Gold
LHb
LPO
b
-3.12
-3.60
-4.16
-3.30
-3.80
c
20 µm
d
Number of LHb-projecting cells
200
150
100
50
0
- MOR+/FG+
- MOR–/FG+
LPO
MPO/AHA
VP
HDB
BNST
EAC
e
Proportion of MOR+ Inputs to LHb
LPO
MPO/AHA
VP
HDB
BNST
EAC
f
- MOR+/FG+
- MOR–/FG+
+0.62
+0.38
+0.14
-0.10
-0.46
-0.82

Figure 5

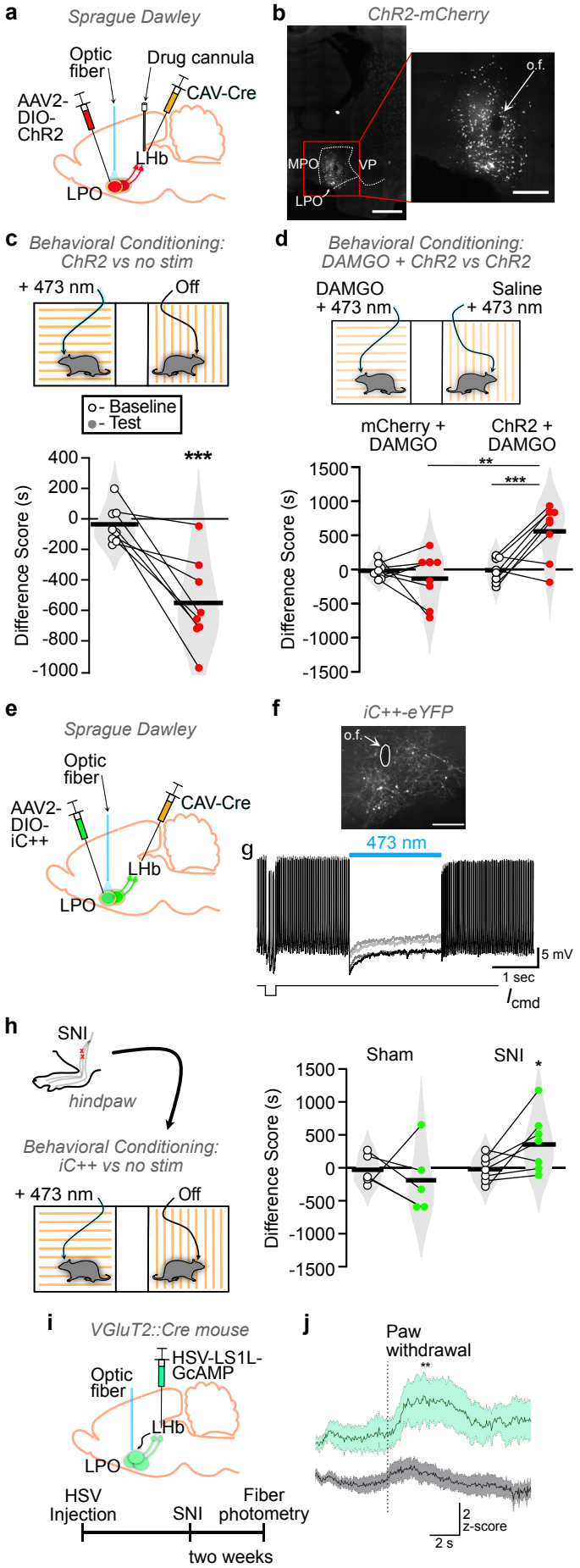
a
Sprague Dawley
Optic fiber
Drug cannula
AAV2-DIO-ChR2
CAV-Cre
LHb
LPO
b
ChR2-mCherry
o.f.
MPO
VP
LPO
c
Behavioral Conditioning: ChR2 vs no stim
+ 473 nm
Off
Baseline
Test
Difference Score (s)
***
d
Behavioral Conditioning: DAMGO + ChR2 vs ChR2
DAMGO + 473 nm
Saline + 473 nm
mCherry + DAMGO
ChR2 + DAMGO
**
***
Difference Score (s)
e
Sprague Dawley
Optic fiber
AAV2-DIO-iC++
CAV-Cre
LHb
LPO
f
iC++-eYFP
o.f.
g
473 nm
5 mV
1 sec
I cmd
h
SNI
hindpaw
Behavioral Conditioning: iC++ vs no stim
+ 473 nm
Off
Sham
SNI
*
Difference Score (s)
i
VGluT2::Cre mouse
HSV-LS1L-GcAMP
Optic fiber
LHb
LPO
HSV Injection
SNI
Fiber photometry
two weeks
j
Paw withdrawal
**
2 z-score
2 s

Figure 6

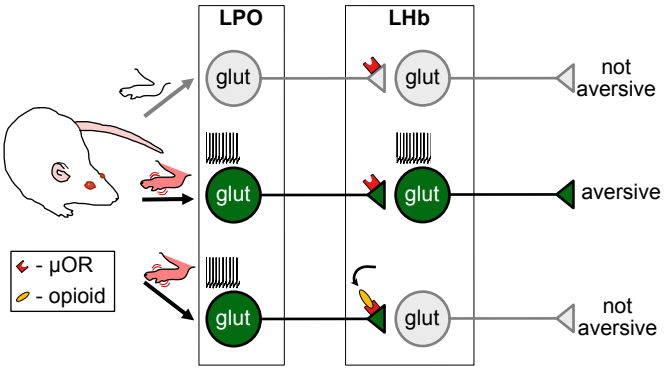
LPO
LHb
glut
glut
glut
glut
glut
glut
not aversive
aversive
not aversive
- μOR
- opioid

Extended Data Figure 1

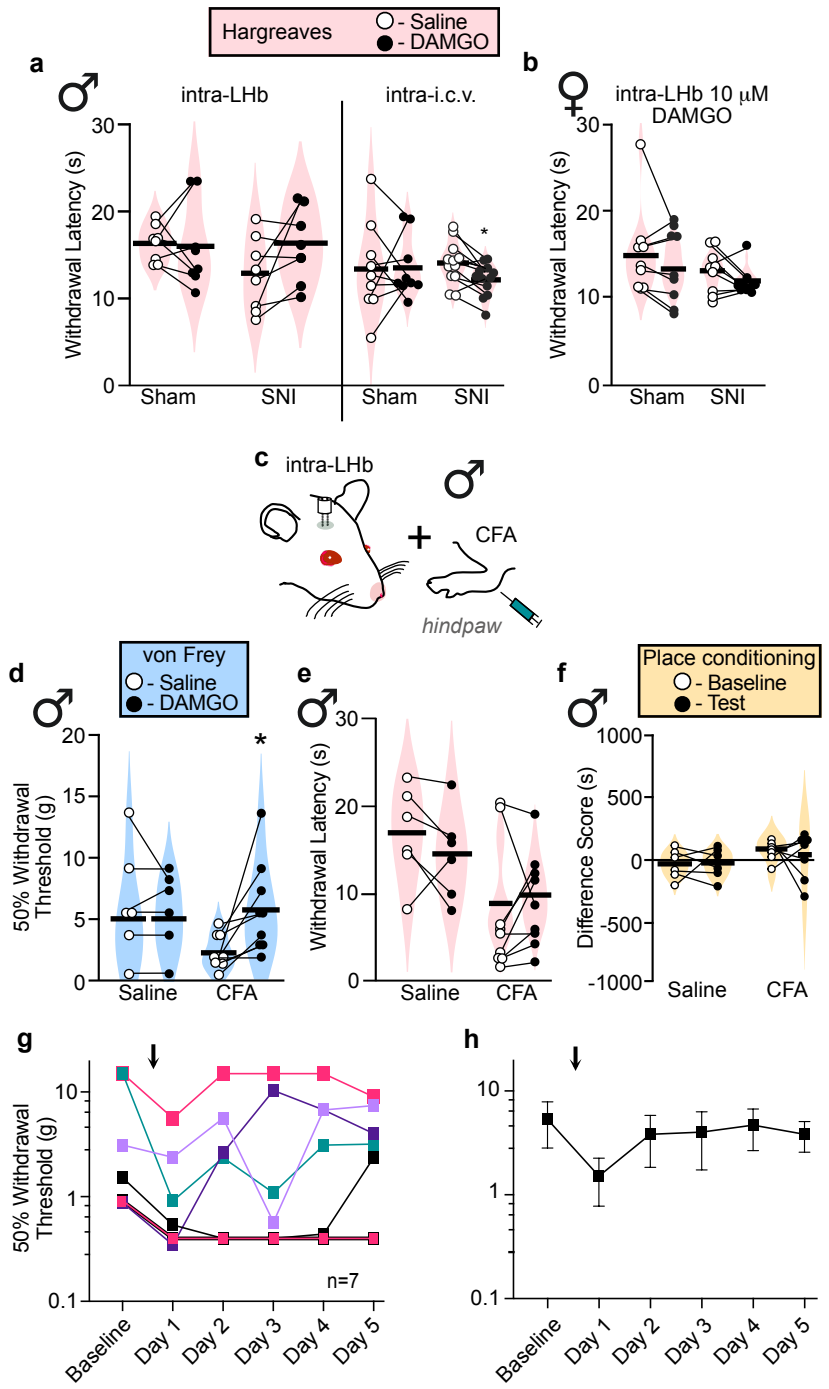

Extended Data Figure 1. *Further characterization of neuropathic pain and inflammatory pain models and the impact of intra-LHb MOR activation in rat.* **a,** (Left) Violin plots of withdrawal latency to heat in male sham (n = 9) and SNI (n = 8) rats with SNI after saline vs DAMGO (10 μM) microinjections into the LHb. Two-way mixed ANOVA revealed no significant interaction between injury and drug condition ($F(1,14) = 2.522$, $p = 0.135$) in the intra-LHb male cohort (Left). Bonferroni corrected paired t test was conducted between drug conditions for normally distributed Sham (Sham males: $p = .861$) and SNI (SNI males: $p = 0.096$) animals. Two-way mixed ANOVA indicated no significant interaction between injury and drug condition ($F(1,19) = 1.549$, $p = 0.228$) in male intra-i.c.v. cohort (Right). Sham animals were non-parametrically distributed, the Wilcoxon signed rank test was conducted ($V = 24$, $p = 0.9102$) while SNI animals were normally distributed, and a Bonferroni corrected paired t test was conducted ($p = 0.0433$). **b,** Two-way mixed ANOVA indicated no significant interaction between injury and drug condition ($F(1,16) = 0.008$, $p = 0.929$). Both the Sham and SNI female groups were non-parametrically distributed, the Wilcoxon signed rank test was conducted, both conditions yielding non-significant differences ($V = 13$, $p = 0.3008$). **c,** To test if the effects of MOR activation in the LHb generalize to other forms of pain, we repeated the manipulations above with an inflammatory model of pain. Male rats received an intradermal injection of CFA or sterile saline into the plantar aspect of the hindpaw. Schematic diagram of inflammatory injury preparations and cannulation targeting the LHb. **d**, Mechanical withdrawal thresholds in sham and CFA-injured rats. In animals with CFA, we observed an increase in the average withdrawal threshold following intra-LHb DAMGO (10 μM) compared to saline, indicating a reduction in mechanical allodynia: Two-way mixed ANOVA revealed significant injury and drug condition interaction ($F(1,13) = 5.772$, $p = 0.032$) with Bonferroni corrected paired t-test, SNI $p = 0.0178$; saline $p = 0.796$. **e**, Withdrawal latency to heat. DAMGO in the LHb did not reverse the CFA-induced decrease in withdrawal latency to heat. Two-way mixed ANOVA revealed no significant injury and drug condition interaction ($F(1,13) = 2.589$, $p = 0.132$). Bonferroni corrected pair t tests were conducted; saline: $p = 0.455$; CFA: Wilcoxon signed rank test, $V = 33$, $p = 0.25$. **f**, Rats with CFA injury also did not develop a preference to intra-LHb DAMGO in the place conditioning paradigm: Two-way mixed ANOVA, no significant interaction between CFA/saline and baseline/test $F(1,11) = 0.104$, $p = 0.753$. Bonferroni corrected t tests were conducted between drug conditions for saline (saline: $p = 0.901$) or CFA (CFA: $p = 0.706$) treated animals. The discrepancy between place conditioning results of our neuropathic and inflammatory pain animals may be due to the natural history of the injury caused in the CFA model: whereas SNI animals underwent permanent nerve ligation, animals injected with CFA presented with transient swelling and erythema of the hindpaw. Within a few days of CFA injection, this phenotype had resolved in our rats. **g,** Mechanical allodynia also reversed quickly: in a separate cohort of rats, all subjects displayed a sharp decline in withdrawal threshold from baseline on day 1 following CFA injection, but the injury-induced allodynia returned to control levels by day 5 in many animals. Individual animals were tested daily; each line represents a male rat. **h,** Average across rats shows that our CFA-induced reduction in mechanical allodynia reversed within a few days. Since our place conditioning training exceeds this time window, resolution of the injury probably occurred before training was completed, thus preventing the formation of a robust association between pain relief and place conditioning apparatus context to produce a CPP. Circles or squares indicate individual animals, while connecting lines indicate within-subject manipulations. $^*p \leq 0.05$

Extended Data Figure 2

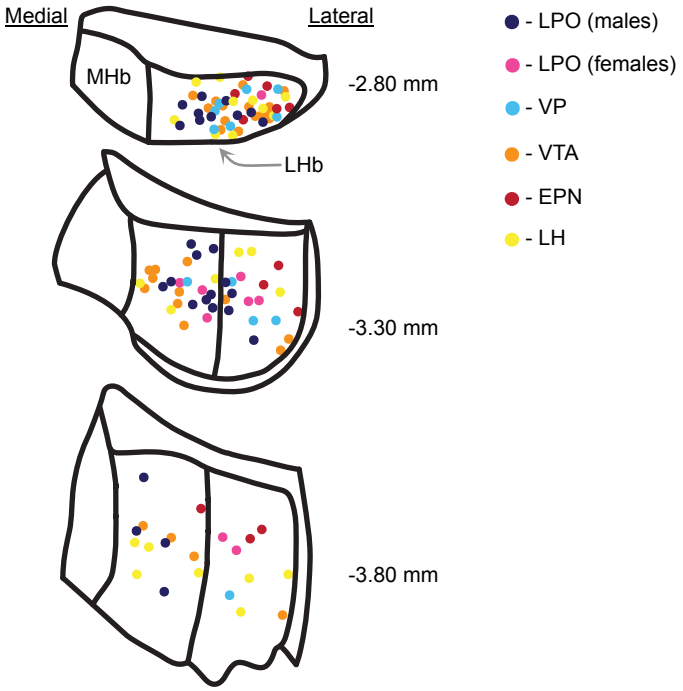

Extended Data Figure 2. *Neurons receiving functional synaptic inputs from the five brain regions showing connectivity were distributed throughout the LHb.* Locations of neurons with functional synaptic connections detected using whole-cell recordings from optogenetic stimulation of terminals arising from each input tested. Locations are based on a combination of biocytin immunohistochemistry localization and low magnification visualization of the cell location during recording. Color indicates source of innervation.

Extended Figure 3

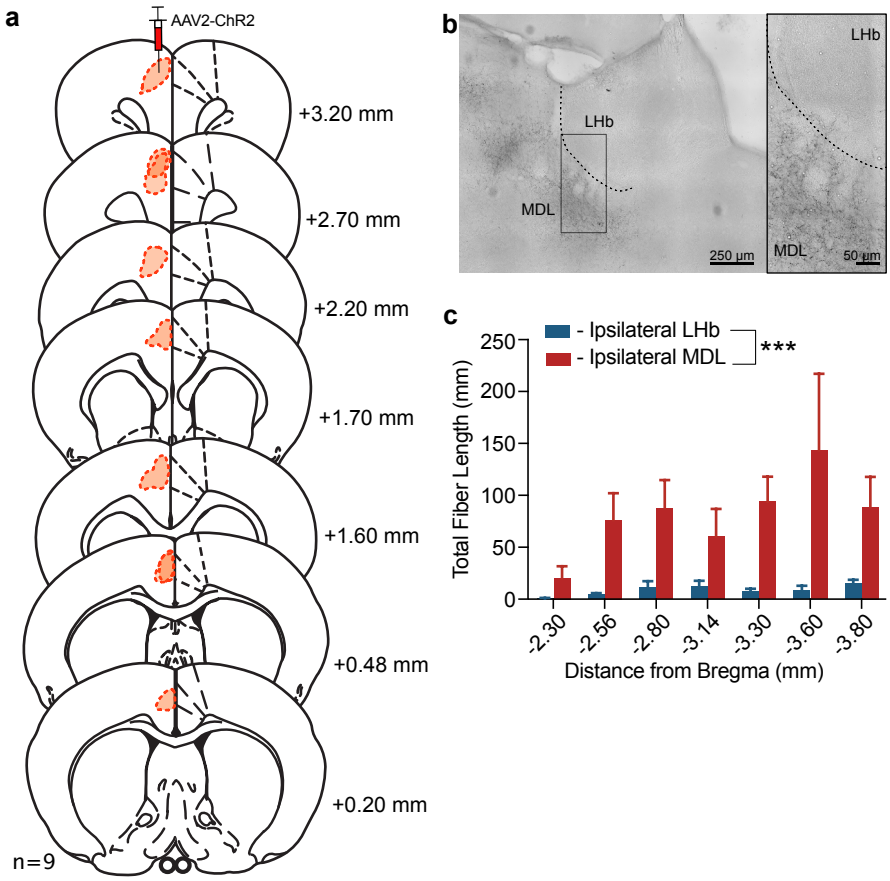

Extended Data Figure 3. *ACC minimally innervates the LHb.* **a**, Diagram of the extent of unilateral AAV2-hSyn-hChR2(H134R)-mCherry injection sites (n = 9 male rats) throughout anteroposterior range of the ACC for anterograde tracing study. **b,** Example ipsilateral DAB-positive fibers (black) visualized under brightfield illumination. Fibers heavily innervate the MDL, which abuts the lateral edge of the LHb, while sparse to no fibers innervate the LHb. Contralateral innervation of LHb and MDL was negligible compared to the ipsilateral side, and therefore were omitted from our analysis. (Left) Scale bar = 250 µm. (Right) Scale bar = 50 µm. **c**, Average stereologically-quantified DAB-positive fiber lengths throughout anteroposterior range of the LHb, compared to the MDL innervation in the same coronal slice. Mann-Whitney test, two-tailed: U = 0, p = 0.0006.

Extended Data Figure 4

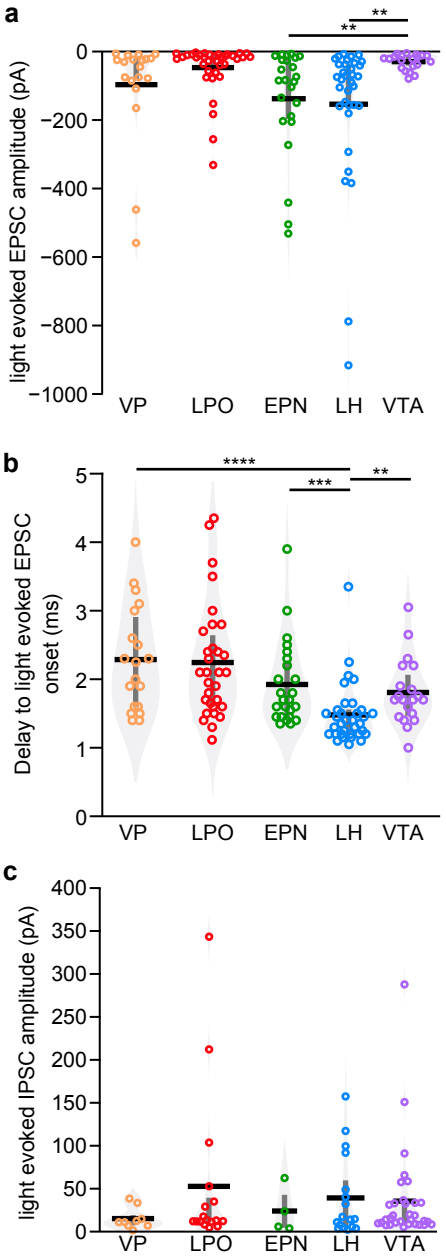

Extended Data Figure 4. *Sources of glutamatergic inputs to the rat LHb vary in strength and delay in synaptic transmission.* **a**, We observed some variations between inputs in the mean light evoked EPSCs (V_m = -60 mV). In particular, excitatory inputs from the VTA were consistently small: Kruskal-Wallis $\chi 2$ = 25.5, df = 4, p = 0.00004, followed by Dunn Test for pairwise comparisons. **b**, Differences were also detected in the delay to the onset of light evoked EPSCs to LHb neurons from these different sources, with inputs from LH showing the fastest response. Although these data deviate from a normal distribution (Shapiro's test, p = 0.0000001), KDEs (violins) are consistent with continuous distributions, suggesting reliable polysynaptic events were rarely detected. **c**, We observed some variations between inputs in the mean light evoked IPSCs (V_m = -40 mV). While there were no statistically significant differences in amplitudes detected, the mean inhibitory input from the VP was particularly small: Kruskal-Wallis $\chi 2$ = 2.3, df = 4, p = 0.7. ** p < 0.01, *** p < 0.005, **** p < 0.0005

Extended Data Figure 5

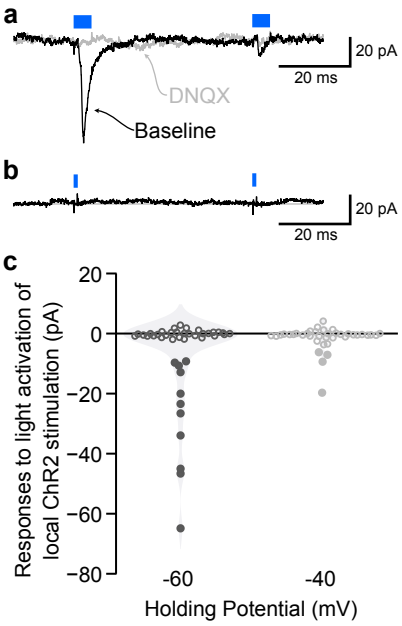

Extended Data Figure 5. *Optogenetic experiments detect local glutamate, but not GABA, functional connections in rat LHb.* AAV2-hSyn-hChR2(H134R)-mCherry was stereotaxically injected into the LHb at least 4 weeks prior to *ex vivo* whole cell recordings in the LHb to detect local synaptic connections. Neurons were recorded blind to ChR2 expression, therefore in some cases the patched neuron expressed ChR2. Therefore, in addition to connectivity criteria used for other afferent inputs, in these experiments only light evoked inward currents that were blocked by 10 μM DNQX were considered glutamatergic connections, and direct ChR2 induced inward currents were subtracted out for the quantification illustrated here. Each cell was probed for both glutamate and GABA inputs in voltage clamp by holding neurons at V_m = -60 mV and -40 mV, light pulse durations 1, 5, and 10 ms durations. **a**, Example recording at V_m = -60 mV showing a light evoked response that was blocked by DNQX. **b**, Example recording at V_m = -40 mV with minimal outward current response within 7 ms of light pulse. This example is the largest outward deflection from baseline observed in these experiments. **c**, Summary of all LHb recordings tested in this experiment. Filled circles represent cells where responses could be classified as local ChR2 induced synaptic transmission. When no clear response was detected, the measure indicated is the difference between the mean $I_{holding}$ of the baseline 100 ms period just prior to the light pulse and the mean $I_{holding}$ 2 ms period starting 2 ms after initiation of the light pulse, consistent with monosynaptic delay timing. None of the recordings made at V_m = -40 mV met the criteria for a response to light stimulation with an outward current.

Extended Data Figure 6

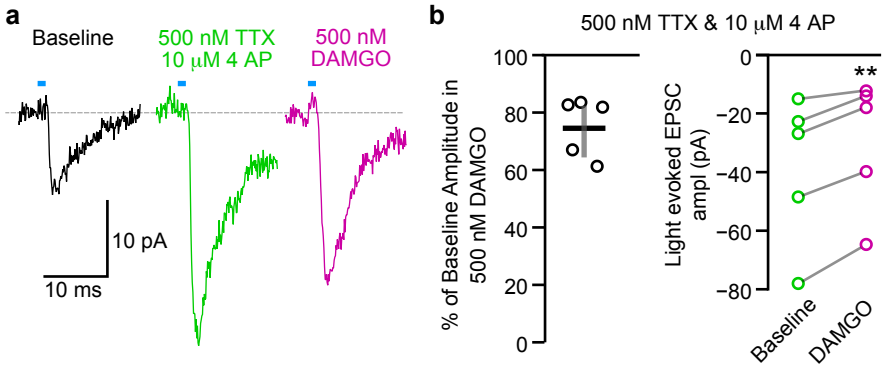

Extended Data Figure 6. *Isolated monosynaptic glutamatergic inputs from LPO to LHb neurons are inhibited by MOR activation.* **a,** Example light evoked EPSC responses in an LHb neuron from a rat with ChR2 expression in LPO neurons. This response persisted in monosynaptic isolation by 500 nM TTX and 100 μM 4 AP (green), and this isolated response was inhibited by 500 nM DAMGO (magenta). **b**, Summary of DAMGO effects on isolated monosynaptic EPSC inputs to LHb neurons expressed as % of baseline monosynaptic response (left) and as raw EPSC magnitudes (right). Paired t-test, df = 4, t = -5.1, p = 0.007. ** $p < 0.01$

Extended Data Figure 7

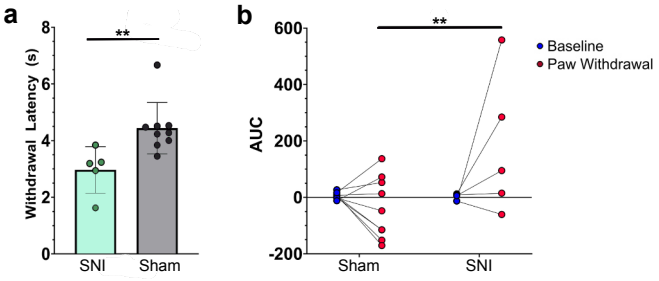

Extended Data Figure 7. *Mice with SNI show hypersensitivity to heat and increased activity in LHb-projecting LPO neurons during paw withdrawal from thermal stimulation.* **a,** Mice with SNI show a reduced latency to withdraw their paw following thermal stimulation in the Hargreaves task. Unpaired t-test, $t(12) = 3.007$, $p = 0.011$. **b,** VGluT2-expressing LPO neurons that project to the LHb expressed GCaMP6m and showed a greater calcium response during paw withdrawal to Hargreaves thermal stimulation (area under the curve, deviation from baseline fluorescence) in SNI animals (n = 5) compared to sham controls (n = 9): Two-way ANOVA, $F(1,12) = 5.4$, $p = 0.038$; Holm-Sidak post-hoc test, $p = 0.0074$. ** $p < 0.01$

Extended Data Figure 8

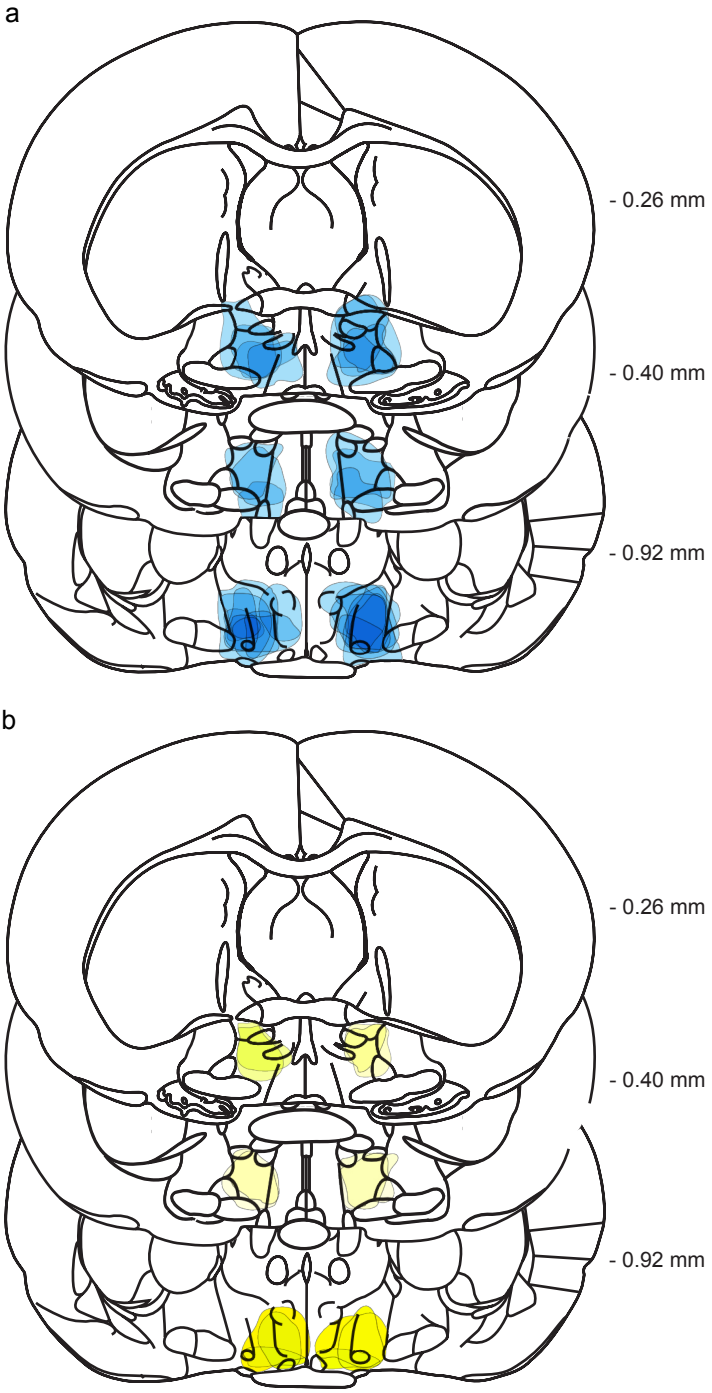

Extended Data Figure 8. Locations and spread of bilateral ChR2 (a) and iC++ (b) expression in the LPO in rats used for *in vivo* optogenetic experiments in Fig 5.